

1                                   **Lamina cribrosa hypoxia sensitivity**  
2                                   **to variations of anatomy and vascular factors**

3                                   Yuankai Lu <sup>1</sup>, Yi Hua <sup>1,3,4</sup>, Po-Yi Lee <sup>1,2</sup>,

4                                   Andrew Theophanous <sup>2</sup>, Shaharoz Tahir <sup>2</sup>, Qi Tian <sup>2</sup>, Ian A. Sigal <sup>1,2\*</sup>

5  
6                                   <sup>1</sup> Department of Ophthalmology, University of Pittsburgh, Pittsburgh PA, USA

7                                   <sup>2</sup> Department of Bioengineering, University of Pittsburgh, Pittsburgh PA, USA

8                                   <sup>3</sup> Department of Biomedical Engineering, University of Mississippi, University, MS, USA

9                                   <sup>4</sup> Department of Mechanical Engineering, University of Mississippi, University, MS, USA

**Short title:** Factors influencing LC oxygenation

**\* Correspondence:**

Ian A. Sigal, Ph.D.

Laboratory of Ocular Biomechanics

Department of Ophthalmology,

University of Pittsburgh Medical Center, UPMC Mercy Pavilion, 1622

Locust St. Rm. 7.382, Pittsburgh, PA 15219, USA;

**Keywords:** glaucoma, lamina cribrosa, vasculature, hemodynamics, oxygenation, blood flow

**Conflict of Interest:** none

**Funding:** National Institutes of Health R01-EY023966, R01-EY031708, R01-HD083383, P30-EY008098 and T32-EY017271 (Bethesda, MD), the Eye and Ear Foundation (Pittsburgh, PA), Research to Prevent Blindness (unrestricted grant to UPMC ophthalmology, and Stein innovation award to Sigal IA) and BrightFocus Foundation.

10 **Abstract**

11 Insufficient oxygenation in the lamina cribrosa (LC) may contribute to axonal damage and  
12 glaucomatous vision loss. To understand the range of susceptibilities to glaucoma, we aimed to  
13 identify key factors influencing LC oxygenation and examine if these factors vary with anatomical  
14 differences between eyes. We reconstructed 3D, eye-specific LC vessel networks from  
15 histological sections of four healthy monkey eyes. For each network, we generated 125 models  
16 varying vessel radius, oxygen consumption rate, and arteriole perfusion pressure. Using  
17 hemodynamic and oxygen supply modeling, we predicted blood flow distribution and tissue  
18 oxygenation in the LC. ANOVA assessed the significance of each parameter. Our results showed  
19 that vessel radius had the greatest influence on LC oxygenation, followed by anatomical variations.  
20 Arteriole perfusion pressure and oxygen consumption rate were the third and fourth most  
21 influential factors, respectively. The LC regions are well perfused under baseline conditions.  
22 These findings highlight the importance of vessel radius and anatomical variation in LC  
23 oxygenation, providing insights into LC physiology and pathology. Pathologies affecting vessel  
24 radius may increase the risk of LC hypoxia, and anatomical variations could influence  
25 susceptibility. Conversely, increased oxygen consumption rates had minimal effects, suggesting  
26 that higher metabolic demands, such as those needed to maintain intracellular transport despite  
27 elevated intraocular pressure, have limited impact on LC oxygenation.

28

## 29 1. Introduction

30 Millions of people worldwide suffer from blindness or reduced vision due to glaucoma, a disease  
31 characterized by the degeneration of retinal ganglion cells and their axons.<sup>1,2</sup> In glaucoma, axonal  
32 damage is widely believed to initiate at the lamina cribrosa (LC) region within the optic nerve head  
33 (ONH);<sup>3,4</sup> however, alternative hypotheses suggest that damage may begin at the neuroretinal  
34 rim<sup>5</sup> or within the brain.<sup>6</sup> The LC receives blood with nutrients and oxygen through a complex  
35 and dense vascular network that is intertwined with the collagen beams and the retinal ganglion  
36 cell axons<sup>7-11</sup> Although the precise mechanisms of axon damage in LC remain unclear, one of  
37 the leading hypotheses posits that insufficient perfusion and oxygenation within the LC may  
38 contribute to cause the axonal damage.<sup>12-17</sup>

39 The LC microcirculation could be influenced by various factors, including vascular network  
40 geometry, perfusion blood pressure, tissue metabolic demands, tissue deformations,  
41 autoregulation responses, and tissue remodeling mechanisms.<sup>8, 18-20</sup> These factors could act  
42 independently or interact with each other, impacting both tissue perfusion and oxygenation, and  
43 thereby influencing physiological and pathological scenarios. Moreover, elevated intraocular  
44 pressure (IOP), one of the primary risk factors for glaucoma, could also contribute to this process.  
45 Elevated IOP can lead to deformation, compression, and distortion of the LC vasculature,  
46 compromising blood and oxygen supply to the LC region.<sup>14, 19, 21-23</sup> Our previous work also showed  
47 that LC oxygenation is more susceptible to systematic IOP-induced deformation than stochastic  
48 vasculature damage.<sup>24</sup> However, the critical threshold of IOP for glaucoma varies among patients  
49 and many individuals with elevated IOP never suffer full vision loss due to glaucoma.<sup>25</sup> To address  
50 the variation among different eyes and identify the most influential factors, a systematic analysis  
51 involving multiple eyes and various potential risk factors affecting LC hemodynamics and  
52 oxygenation is necessary. Such systematic investigations are crucial for advancing our  
53 understanding of glaucoma pathophysiology and developing more effective diagnostic and  
54 therapeutic strategies.

55 Despite major advances of imaging techniques over the last several years, such as optical  
56 coherence tomography angiography (OCT-A)<sup>26-29</sup>, ultrasound techniques<sup>30</sup>, MRI-based  
57 techniques<sup>31</sup>, and laser speckle flowgraphy (LSFG)<sup>32</sup>, obtaining direct measurements of LC  
58 hemodynamics and oxygenation with adequate resolutions and depth penetration remains elusive.  
59 Therefore, alternative approaches, such as theoretical modeling and numerical simulations, have  
60 been employed to assess blood flow and oxygenation within the LC region.<sup>14, 15, 21, 24, 33, 34</sup> Recently,  
61 we utilized experimentally-derived reconstructed 3D model of eye-specific LC vasculature and  
62 computational techniques for analyzing hemodynamics and oxygenation, and their influential  
63 factors.<sup>34</sup> We found that vessel radius, oxygen consumption rate, and arteriole perfusion pressure  
64 were the three most significant factors influencing LC oxygenation. However, the study was  
65 preliminary and based on a single eye anatomy. Eyes, however, vary in anatomy and a result  
66 applicable to one eye is not necessarily exactly the same for another. Hence, it remains unclear  
67 whether the factor influences identified on our previous study generalize to other eyes.

68 Our goal in this study was to identify the most influential factors and address the impact of eye  
69 anatomy differences on LC oxygenation. To achieve our objective, four eye-specific 3D models  
70 of the LC vasculature were reconstructed based on histological sections. From this, numerical  
71 simulations were performed to evaluate LC hemodynamics and oxygenation. Specifically, we  
72 parameterized the vessel radius, oxygen consumption rate, and arteriole perfusion pressure to  
73 evaluate their impact on LC oxygen supply. We used a regularized grid to generate parameter  
74 combinations, allowing for the analysis of the independent and correlated effects of each  
75 parameter.

76

77

## 78 **2. Methods**

79 *General procedure.* First, we labeled, imaged, and reconstructed the eye-specific ONH  
80 vasculatures of four healthy monkeys as our baseline models, following the technique described  
81 elsewhere.<sup>35, 36</sup> Based on the four baseline vascular network models we then created 500 models  
82 by varying vessel radius, neural tissue oxygen consumption rate and arteriole blood pressure  
83 (four eyes, five levels per parameter, three parameters:  $4 \times 5^3 = 500$ ). Second, we performed  
84 hemodynamics and oxygenation simulations to evaluate the blood supply and from this the  
85 oxygen field within the ONHs. Third, we compared the fraction of hypoxic regions and the  
86 minimum oxygen tension within the LC across all models to determine the factor influences on  
87 LC hemodynamics and oxygenation. The steps are described in detail below.

### 88 **2.1 Reconstruction of 3D eye-specific LC vascular network**

89 All procedures were approved by the University of Pittsburgh's Institutional Animal Care and Use  
90 Committee (IACUC), and followed both the guidelines set forth in the National Institute of Health's  
91 Guide for the Care and Use of Laboratory Animals and the Association of Research in Vision and  
92 Ophthalmology (ARVO) statement for the use of animals in ophthalmic and vision research.

#### 93 *Vessel labeling.*

94 We processed four healthy female rhesus macaque monkeys' heads for vessel labeling. The  
95 animals were raised under similar conditions. The ages of the monkeys at the time of sacrifice  
96 were 15, 16, 14, and 13 years for eyes 1, 2, 3, and 4, respectively. Within two hours after sacrifice,  
97 we cannulated the anterior chamber of each eye to control IOP throughout the experiment. IOP  
98 was set to 5 mmHg to prevent hypotony or hypertension. Two polyimide microcatheters were  
99 inserted into the carotid arteries for labeling. Warm phosphate-buffered saline (PBS) was  
100 perfused to wash out intravascular blood first. A lipophilic carbocyanine dye, Dil, was then used  
101 to label the vessels in the eye. We perfused 100 ml Dil solution into each carotid artery, followed  
102 by a 100ml 10% formalin perfusion to fixate the eye.

103 *Histology and 3D vasculature reconstruction.*

104 The ONH and surrounding sclera were then isolated, cryoprotected, and sectioned<sup>37</sup>. Each  
105 section underwent imaging through Fluorescence Microscopy for vessel visualization and  
106 Polarized Light Microscopy for collagen visualization.<sup>35, 38</sup> 3D vasculature reconstruction involved  
107 importing and registering sequential these images in Avizo software (version 9.1). Vessel  
108 segmentation aided by a Hessian filter, and vessels in the LC region were identified by the  
109 presence of collagen beams.<sup>35</sup> Our reconstructed vascular networks included the whole LC region,  
110 and some of the pre-laminar and retro-laminar regions (Figure 1). This ensured that the 3D LC  
111 network was fully enclosed within the region reconstructed.

112 *Vessel diameter setting.*

113 Although our reconstruction technique could be leveraged to obtain the vessel diameter  
114 information, we acknowledge that post-mortem changes, tissue swelling, and pressure variations  
115 can alter vessel diameters from in vivo conditions. Autoregulation, particularly in the deep optic  
116 nerve head (ONH) and lamina cribrosa (LC), remains uncharacterized in vivo. Following previous  
117 studies of LC hemodynamics<sup>14, 15, 24, 33, 34</sup>, we assumed that all vessels in the LC had the same  
118 diameter. A uniform capillary radius of 4  $\mu\text{m}$  was selected based on prior measurements<sup>39</sup>, as  
119 discussed in<sup>34</sup>. Further research, combining our technique with in vivo imaging, could improve  
120 our understanding of vessel diameters and autoregulation in the LC.

121 *Vascular reconstruction validation.*

122 The post-mortem dye perfusion process may encounter challenges, such as incomplete  
123 penetration into all vessel segments due to intravascular clotting or insufficient perfusate volume.  
124 To reduce clotting, we minimized the interval between animal death and perfusion and thoroughly  
125 washed the ONH with PBS. Our imaging revealed strong signals in retinal and choroidal vessels,  
126 indicating successful perfusion and sufficient labeling. Nevertheless, we acknowledge that vessel  
127 visualization and reconstruction could be impacted by uneven labeling, discontinuities, or leaks.  
128 Manual corrections, including 'cleaning' and 'bridging' segments, were performed to address

129 these issues, though they may introduce artifacts and randomness.<sup>34, 35</sup> To evaluate the  
130 reconstruction technique, two students independently reconstructed the same labeled eye, and  
131 their results were compared to assess the method's validity. Reconstruction 1 and Reconstruction  
132 2 represent the two independent reconstructions of the same eye. The total vessel lengths for  
133 Reconstruction 1 and Reconstruction 2 were 547.68 mm and 528.68 mm, respectively, differing  
134 by only 3.3%. The average LC oxygen partial pressures were 55.56 mmHg and 54.85 mmHg, a  
135 difference of 1.3%.

136 Figure 2 illustrates the vessel geometry and oxygenation difference of Reconstruction 1 and  
137 Reconstruction 2, where the shared vasculature (yellow) included 9584 segments.  
138 Reconstruction 1 included 1334 unique segments, and Reconstruction 2 included 859 unique  
139 segments. The shared vasculature accounts for approximately 90% of the total vessels in both  
140 models. The oxygenation differences were minimal, further demonstrating the high repeatability  
141 of the reconstruction process.

## 142 **2.2 Hemodynamics and Oxygenations**

### 143 Oxygen diffusion in tissue

144 We followed the approach described in <sup>40</sup> to perform the LC hemodynamics and oxygenation  
145 simulations. Oxygen transport within the oxygen-consuming neural tissues can be described by  
146 the reaction-diffusion equation <sup>41</sup>:

$$147 \quad D\alpha\Delta P_{O_2} = M(P_{O_2}),$$

$$148 \quad M(P_{O_2}) = M_0 P_{O_2} / (P_0 + P_{O_2}),$$

149 where D is the oxygen diffusion coefficient,  $\alpha$  is the oxygen solubility coefficient, and  $P_{O_2}$  is the  
150 tissue oxygen partial pressure. The oxygen consumption term  $M(P_{O_2})$  can be estimated by  
151 Michaelis-Menten enzyme kinetics <sup>41</sup>, where  $M_0$  represents oxygen demand and  $P_0$  is the oxygen  
152 partial pressure at half-maximal consumption. In this study,  $M_0$  was assumed to be uniform  
153 throughout the LC.

### 154 Oxygen flux in blood

155 ONH vascular network system was considered as a set of interconnected capillary elements. The  
156 capillary elements connect with each other at the bifurcation nodes. The blood flow within a  
157 capillary can be approximately by the Poiseuille flow due to the low Reynolds number ( $< 0.05$ ) <sup>42</sup>,

$$158 \quad Q = \frac{\pi r^4}{8\mu L} \Delta P,$$

159 where Q is the flow rate, r is the vessel radius, L is the vessel length,  $\mu$  is the blood viscosity, and  
160  $\Delta P$  is the pressure drop along the vessel. The blood viscosity  $\mu$  was described as a function of  
161 vessel radius and hematocrit (i.e., the volume fraction of red blood cells). The behavior of red  
162 blood cell flow in small vessels is complex and beyond the scope of this study, but readers are  
163 encouraged to read the papers by Pries and Secomb (Pries et. al., 2008) and by Ebrahimi and  
164 Bagchi (Ebrahimi et al., 2022). A detailed description of the effective viscosity is provided in the

165 Appendix. For a baseline vessel diameter of 8  $\mu\text{m}$ , the effective viscosity was approximately  
166  $7.65 \times 10^{-3} \text{ mPa}\cdot\text{s}$  in this work

### 167 Blood pressure boundary conditions

168 The model boundaries were divided into four regions for assigning the blood pressure conditions  
169 that drive the blood flow throughout the vascular network (Figure 1).

170 At the periphery: An arteriole pressure of 50 mmHg was set as baseline to represent blood inflow  
171 from the circle of Zinn-Haller.<sup>14, 15</sup>

172 At the center: A venule pressure of 15 mmHg was set as baseline to represent blood drainage  
173 through the central retinal vein.<sup>14, 15, 43</sup>

174 Many previous studies of LC hemodynamics assumed no flow through the anterior and posterior  
175 LC boundaries, either explicitly or by assuming no vessel interconnections.<sup>15, 44</sup> Our  
176 reconstructions show a large number of interconnections<sup>35, 45</sup> and therefore we knew that we had  
177 to develop a new approach. We reasoned that the capillaries should remain open under normal  
178 conditions. This, in turn, required blood pressure to exceed the surrounding tissue pressure. Thus,  
179 for each boundary we estimated the “worst-case” blood pressure based on the tissue pressure  
180 levels, which then differed for the anterior and posterior boundaries.

181 Anterior Boundary: Prelaminar tissues are highly compliant, with minimal pressure drop, so tissue  
182 pressure was set equal to IOP (15 mmHg). Based on experimental<sup>46</sup> and numerical studies<sup>47</sup>, a  
183 blood pressure of 20 mmHg was assigned for the anterior boundary, considering a 5 mmHg  
184 fluctuation due to the cardiac cycle.

185 Posterior Boundary: The tissue pressure behind the LC, sometimes referred to as the retrolaminar  
186 tissue pressure (RLTP), is related to, but not identical to, cerebrospinal fluid pressure (CSFP).  
187 Based on Morgan et al.,<sup>46</sup> RLTP can be approximated as  $0.82 \times \text{CSFP} + 2.9 \text{ mmHg}$ . Assuming  
188 a CSFP of 10 mmHg,<sup>48, 49</sup> the estimated RLTP is 11 mmHg. The average posterior boundary

189 blood pressure was set at 16 mmHg to prevent capillary collapse, considering a 5 mmHg cardiac  
190 cycle fluctuation.

191 Human retinal vein branches, with diameters ranging from 33.3 to 155.4  $\mu\text{m}$ , exhibit blood flow  
192 velocities of 19.3 mm/s.<sup>50</sup> The mouse central retinal artery, ophthalmic artery, and long posterior  
193 ciliary artery have velocities of 20–30 mm/s<sup>51</sup>, while human central retinal arteries exhibit  
194 velocities of 15–35 mm/s<sup>52</sup>. 15 mm/s was considered to be characteristic of arterial flow and thus  
195 unphysiological for capillaries, this corresponds to a threshold of 45 nl/min in our baseline  
196 condition.

197 The oxygen flux in blood vessels satisfies:

$$198 \quad f(P_b) = Q(\alpha_{\text{eff}}P_b + H_D C_0 S(P_b)),$$

199 Where  $Q$  is the flow rate,  $\alpha_{\text{eff}}$  is the effective solubility of oxygen in plasma,  $H_D$  is the hematocrit,  
200  $C_0$  is the concentration of hemoglobin-bound oxygen in a fully saturated red blood cell,  $P_b$  is the  
201 blood oxygen partial pressure (mmHg),  $S(P_b)$  is the oxygen-hemoglobin saturation, determined  
202 by the empirical oxygen–hemoglobin dissociation curve.

### 203 Oxygen exchange on vessel walls

204 Conservation of oxygen along each vessel segment implied that,

$$205 \quad \frac{df(P_b)}{ds} = -q(s),$$

206 where  $s$  is arc-length parameter along the vessel, and  $q(s)$  is the total oxygen flux through the  
207 blood vessel wall per unit vessel length.

208 At the interface between blood vessel and tissue, the diffusive oxygen flux across the vessel wall  
209 must be consistent with the surrounding tissue oxygenation, implying that,

$$210 \quad q(s) = -D\alpha \int_0^{2\pi} \frac{\partial P_{O_2}}{\partial r} R d\theta,$$

211 where  $r$  is the radial distance from the vessel centerline,  $R$  is the vessel radius, and the integral  
212 is around the circumference, denoted by angle  $\theta$ . Therefore, the oxygen flux can be evaluated  
213 from the average gradient of  $P_{O_2}$  on the vessel wall.

214 As reported before<sup>40</sup>, we used a fast and efficient method to simulate the convective and diffusive  
215 oxygen transport in the complex ONH vascular networks. The method employs an implicit finite-  
216 difference scheme with the multigrid algorithm to compute the tissue oxygen field, while blood  
217 oxygenation is modeled as a system of ordinary differential equations along the vessels. Oxygen  
218 exchange at the vessel wall is incorporated into the tissue oxygen discretization using a numerical  
219 delta distribution function. A physics-based iterative approach ensures convergence and  
220 accuracy of the nonlinear system. We used frequency for both blood flow and oxygenation  
221 analyses. For blood flow, frequency represents the fraction of capillary segments. For oxygenation,  
222 frequency represents the fraction of neural tissue points under the corresponding tissue  
223 oxygenation. All parameters are listed in Table 1.

### 224 **2.3 Parametric analysis**

225 We performed a parametric analysis based on the variation of three parameters: vessel radius,  
226 neural tissue oxygen consumption rate, and arteriole pressures. These parameters were selected  
227 because they had the strongest influences on LC hemodynamics and oxygenation in our previous  
228 study.<sup>34</sup> Baseline values of the parameters were established from the literature, as shown in Table  
229 1 and discussed in detail<sup>34</sup>. To provide a systematic and unbiased parametric analysis these were  
230 all varied  $\pm 20\%$  of the baseline (80% to 120%). Five parameter levels were selected: 80% (low),  
231 90%, 100% (Baseline), 110% and 120% (high), resulting in a total of  $5 \times 5 \times 5 = 125$  models for each  
232 eye. We repeated the same parametric analysis for all four eyes, resulting in a total of 500 models.  
233 As outcome measures, we used the minimal oxygen tension in the LC and the tissue volume  
234 fraction of the hypoxia region<sup>53-55</sup>. For minimal oxygen tension, the 10<sup>th</sup> percentile was used as

235 the definition of the minimal value to reduce the influence of very small regions that could be  
236 artifactual<sup>34</sup>.

237 Tissue hypoxia, characterized by reduced tissue oxygenation, is generally a consequence of  
238 structurally and functionally disturbed microcirculation.<sup>56, 57</sup> We discussed this issue in length in  
239 a previous publication.<sup>24</sup>

240 Hypoxia can be categorized into:

- 241 1) Normoxia: Normal cellular activity and metabolism.
- 242 2) Mild hypoxia: Physiological responses. If sustained chronically, it may contribute to neural  
243 tissue damage.
- 244 3) Severe hypoxia: Tissue necrosis, irreversible damage.

245 This study focuses on parametric evaluation for chronic pathologies, such as glaucoma. To  
246 simplify the analysis, we adopted mild hypoxia as the threshold, as it reflects conditions that may  
247 contribute to chronic injury without immediate tissue necrosis.

248 The hypoxia threshold for ONH is unknown, and could vary from species and individuals. We  
249 conducted a literature survey for normoxia/hypoxia, with the findings summarized below. 8 mmHg  
250 (~1% oxygen) has been consistently used as a threshold for severe hypoxia in neural tissues.<sup>58-</sup>

251 <sup>60</sup> Tissue normoxia, however, varies widely, from 20 mmHg to 50 mmHg, and is difficult to  
252 measure under in-vivo ONH conditions.<sup>56, 60-62</sup> Considering the hypoxia-sensitive neural cells in  
253 the LC region, we analyzed precedents set in existing literature; in the normal ONH and cerebral  
254 cortex.<sup>57, 59, 62, 63</sup> We settled on a threshold of 38mmHg (~5% oxygen) for tissue normoxia, as used  
255 in<sup>54</sup>. We selected a threshold in the upper end of values reported in the literature, reasoning that  
256 it may be more relevant for chronic conditions. Selecting a lower threshold would decrease the  
257 estimates of hypoxic region fraction.

258

259

## 260 **2.4 Statistical analysis**

261 We utilized ANOVA to assess the rank and statistical significance of all parameters. Specifically,  
262 we used the percentage of the total sum of squares corrected by the mean as a metric to represent  
263 the contribution of each parameter and interaction.<sup>17</sup> The results among different eyes were  
264 analyzed collectively, where the eye itself was considered as a categorical factor in ANOVA to  
265 account for individual variations in our models. Further details regarding the statistical analysis  
266 can be found in our previous parametric work.<sup>34</sup>

267

268 **3. Results**

269 The baseline hemodynamics and oxygenation of the four networks are shown in Figure 3.  
270 Although the eyes differed in anatomy, their hemodynamic and oxygenation exhibited similar  
271 characteristics. The flow rate and oxygenation were high at the periphery and low at center. This  
272 pattern is consistent with the blood supply for LC, where blood perfusion is from the periphery,  
273 draining through the central retinal vein. A 3D oxygenation map of Eye 1 is shown in Figure 4.  
274 Flow rates in the vessel network vary significantly in scale. The average flow rate across the four  
275 ONHs at baseline is approximately 3.31 nl/min, with the highest flow reaching 104 nl/min. The  
276 flow rate distribution for Eye 1 is shown in Figure 5, indicating that nearly all ONH flow rates  
277 remain within physiological ranges. Detailed illustrations of flow and oxygen pattern are shown in  
278 Figure 6 and Video 1 (See Supplemental Material).

279 Table 2 summarizes the measurements for the four eyes. Our analysis showed that the average  
280 distance to the nearest vessel was similar for eyes 1 and 2, and was larger for eyes 3 and 4.  
281 However, other parameters, including segment number, branch point number, and tortuosity, did  
282 not follow this grouping pattern. Interestingly, the overall region volumes were smallest for Eyes  
283 3 and 4. This suggests that differences in distance parameter may contribute to the observed  
284 grouping of oxygenation patterns. Nevertheless, LC oxygenation is influenced by multiple factors,  
285 and a larger sample size is necessary to further identify the relationship between vascular  
286 geometry and ONH oxygenation.

287 Figure 7 illustrates oxygenation distribution under various radii, consumption rates, and arteriole  
288 pressures for Eye 1. We selected three levels—low (80%), baseline (100%), and high (120%)—  
289 to show the impact of each parameter on LC oxygenation. Notably, changes in vessel radius  
290 caused the largest changes in LC oxygenation distribution, while variations in other parameters  
291 had comparatively smaller effects.

292 Boxplots of the impact of each factor on the 10th percentile oxygenation and the fraction of  
293 hypoxic regions across all eyes are presented in Figure 8. Vessel radius exhibited the strongest

294 positive relationship with the 10th percentile oxygenation and the strongest negative relationship  
295 with the fraction of hypoxic regions, consistent with the results shown in Figure 7. The statistical  
296 significance of each parameter was evaluated via ANOVA (see Figure 9). The most influential  
297 factors were vessel radius, arteriole pressure, and oxygen consumption rate. There were weak  
298 interactions between these influential factors. Specifically, the interactions between radius and  
299 pressure are illustrated in Figure 10.

300

301

#### 302 **4. Discussion**

303 Our goal was to identify the most influential factors on LC oxygenation, including the impact of  
304 eye to eye anatomical variations. Specifically, we used four eye-specific 3D LC vasculature  
305 models and parameterized the vessel radius, oxygen consumption rate, and arteriole perfusion  
306 pressure to evaluate their impact on LC oxygen levels. The four most influential factors on LC  
307 oxygenation were, from most to least influential: vessel radius, eye anatomy, arteriole perfusion  
308 pressure, and oxygen consumption rate. Our models also showed that the LC was well irrigated  
309 at baseline IOP. Below we discuss the findings in more detail as well as the limitations and other  
310 considerations to keep in mind when interpreting them.

#### 311 **Vessel radius was the most influential factor on the LC oxygenation.**

312 Our models predicted that the vessel radius has the strongest contribution to LC oxygenation,  
313 both for the 10<sup>th</sup> percentile oxygenation and hypoxia region fraction. This can be understood as  
314 follows: Vessel radius plays a crucial role in determining the flow resistance of each vessel  
315 segment, as evidence by the well-known quartic power in Poiseuille's flow formula. By precisely  
316 controlling luminal radius through vessel wall contraction and dilation, this sensitivity can be  
317 leveraged by vascular systems to regulate blood and oxygen supply efficiently. There are,  
318 however, some scenarios in which the high sensitivity to vessel radius could prove problematic to  
319 LC perfusion. For example, IOP-induced deformations can distort the LC tissues, altering the  
320 geometry of the vessels within, altering radius. Substantial experimental evidence supports the  
321 idea that blood perfusion in the ONH decreases and vessel radius reduces with elevated IOP.<sup>15,</sup>  
322 <sup>33, 64-66</sup> Thus, our model predictions are consistent with the literature. Given the complexity of the  
323 LC mechanics and vascular network, predicting the effects of IOP-related deformations on LC  
324 oxygenation is not trivial. Elsewhere we have presented a combined experimental-computational  
325 analysis using models similar to those in this work.<sup>67</sup> We found that moderately elevated IOP can  
326 cause sufficient distortions to the LC vasculature to alter LC hemodynamics and lead to mild

327 hypoxia in a substantial part of the LC. More extreme IOP elevations can lead to severe hypoxia  
328 that is likely to cause more immediate damage to the LC neural tissues.

329 **Eye anatomy variations had the second strongest influence on the LC oxygenation.**

330 Eye anatomy variations refer to the differences in oxygenation between eyes. This means that for  
331 vascular networks modeled with exactly the same parameters and differing only on the vascular  
332 network, the hemodynamics and oxygenation were substantially and significantly different. As  
333 shown in the Results section, the four models formed two groups. See, for example, the plot of  
334 LC oxygenation in Figure 3. The models of Eyes 1 and 2 show similar curves, distinct from the  
335 curves of eyes 2 and 4. It is important for readers to recall that the response curves will change  
336 as other parameters vary, however, the ANOVA results indicate that the changes in the curves  
337 will be similar for all the eyes since there were no significant interactions between eye anatomy  
338 and other parameters. This means that eyes differ in hemodynamics and oxygenation, but that  
339 their sensitivity to changes in other parameters is the same. Thus, while it is still not clear why  
340 some eyes, or their vascular networks, behave differently, there is a common similar sensitivity.  
341 Some eyes may be more susceptible to low oxygenation than others, but it seems to be that this  
342 is not because of a higher sensitivity to the parameters. Our recent work investigated the IOP  
343 effect on LC oxygenation across different eyes.<sup>67</sup> Different eyes anatomy led to different LC  
344 oxygenation. However, the changes of LC oxygenation due to IOP-induced deformation were  
345 similar for all eyes, which also suggest the common sensitivity.

346 Previously we conducted a study similar to this one, using a 3D eye-specific model of the LC  
347 vasculature to evaluate how hemodynamics and oxygenation were affected by varying several  
348 parameters.<sup>34</sup> We found that vessel radius, oxygen consumption rate, and arteriole perfusion  
349 pressure were the three most significant factors influencing LC oxygenation. In that study,  
350 however, we used only one vascular network and therefore were unable to evaluate the effects  
351 of eye anatomy. This is why it was crucial to conduct the study described in this paper.

352 Other studies have looked at variations in LC hemodynamics resulting from differences or  
353 changes in anatomy. Most of these studies have considered the LC as a generic model, varying  
354 parameters such as the LC size, depth and curvature.<sup>14, 15, 33, 44</sup> These studies found that structural  
355 parameters, such as cup depth and LC stiffness, had the most significant influence on LC  
356 oxygenation during IOP elevation. This was followed by perfusion pressure, while other structural  
357 parameters, such as anisotropy and pole size, had a weaker impact on LC oxygenation compared  
358 to perfusion pressure. The ranking of influence strength was analyzed using similar techniques  
359 as presented in Figure 9. Overall, LC structural parameters, or eye anatomy, play a crucial role in  
360 influencing LC oxygenation, which is consistent with our findings in this work.

361 The simplified generic models have several important strengths, as we have discussed elsewhere  
362 <sup>68</sup>, but there are also disadvantages. Generic models can potentially miss core details of the  
363 architecture of a specimen. Also, it is possible that the parameter space considered by the generic  
364 models does not represent the actual variability of eyes, not just in terms of the parameters and  
365 their ranges, but their distributions. If this is the case, the sensitivities may be inaccurate. Further,  
366 it is possible that generic models fail to account properly for model complexity and variability and  
367 thus miss important conditions. This is where the use of eye-specific models reveals an important  
368 strength that we leveraged in this work. Eye anatomy, however, remains a discrete parameter.  
369 Elsewhere we have shown techniques that potentially could be adapted to parameterize eye-  
370 specific models.<sup>34</sup>

### 371 **Arteriole perfusion pressure and oxygen consumption rate ranked third and fourth most** 372 **influential factors on LC oxygenation**

373 Arteriole perfusion pressure and oxygen consumption rate ranked as the third and fourth  
374 influential factors on LC oxygenation. The LC oxygenation was positively associated with the  
375 arteriole perfusion pressure, and negatively associated with the oxygen consumption rate. LC  
376 oxygenation reflects the balance between supply and consumption. Increased perfusion pressure

377 would drive more blood flow across the LC and bring more oxygen to neural tissues. Conversely,  
378 a higher oxygen consumption rate would consume more oxygen in LC, potentially leading to  
379 hypoxia under insufficient supply. Perfusion pressure came from the cardiovascular circulation,  
380 and was affected by the upstream vascular systems and some blood flow regulation mechanism.  
381 Cardiovascular dysfunctions, such as hypo/hypertension, were found to be linked to glaucoma  
382 development.<sup>69-72</sup> It is worth noting that the hypo/hypertension will also induce the remodeling of  
383 vascular structures, such as systemic vasoconstriction (vessel radius reduction), capillary  
384 rarefaction, which may also alter the LC hemodynamics and oxygenations.<sup>73-75</sup> The oxygen  
385 consumption rate in LC varied based on the amount, type, and activity of various cells in neural  
386 tissues, including axons, astrocytes, and other cells, and could even change during the glaucoma  
387 development.<sup>55, 59</sup>

388 From a perspective of physiological mechanisms and biological functions, the perfusion pressure  
389 and consumption rate should directly affect the LC oxygenation, which aligns with our  
390 expectations and findings. Interestingly, they contribute less than the eye anatomy variations.

### 391 **The LC was well irrigated at baseline.**

392 All the eyes were well irrigated under baseline conditions, with less than 15% of the LC volume  
393 suffering low enough oxygenation to be at risk of hypoxia. This is consistent with the idea that  
394 healthy individuals have low risk of LC hypoxia. The result also agrees with our previous work on  
395 the robustness of the LC oxygenation.<sup>24</sup>

396 To the best of our knowledge, this is the first study to conduct parametric analysis based on  
397 multiple 3D eye-specific LC models while accounting for eye anatomy. We combined the  
398 experimental-based reconstructed LC vasculature with highly accurate and efficient numerical  
399 simulation techniques to provide a high-resolution estimation of LC hemodynamics and  
400 oxygenation. Our reconstruction technique enables the creation of multiple LC vascular networks  
401 from histological sections of healthy monkeys, offering high-resolution and accurate structural

402 detail. Utilizing a fast algorithm for hemodynamic and oxygenation simulations, we conducted a  
403 systematic parametric analysis across multiple eyes.

#### 404 **Limitations**

405 It is important to acknowledge the limitations of this study so that readers can consider them when  
406 interpreting our findings. The first limitation is that we used computational modeling. While our  
407 techniques have been tested and verified, much better experimental data is required to consider  
408 the predictions from our models confirmed and validated. The LC is extremely complex and there  
409 are still too many aspects that are not fully understood. Unfortunately, at this time, the  
410 experimental tools and techniques necessary to gather the data necessary do not exist. As  
411 discussed before, the challenges in spatial and temporal resolution and in signal penetration are  
412 not yet overcome. There are promising tools in the horizon, like visible light OCT that may enable  
413 measuring blood oxygenation <sup>28</sup> and super-resolution ultrasound that may allow measuring of  
414 blood flow with high resolution and deep into the ONH. <sup>51</sup>

415 While this study expanded on our previous parametric analysis of LC hemodynamics and  
416 oxygenation by including several eye-specific models, another limitation is that using only four  
417 models is insufficient to fully capture the variability observed in human or monkey eyes. Future  
418 studies with a larger number of eye models, particularly including human eyes, are essential to  
419 better understand this variability.

420 Although we reconstructed the 3D eye-specific LC vasculature model from experimental images,  
421 we recognize that there were gaps between our reconstructed vasculature model and the in-vivo  
422 LC vascular network. A salient one is that we set the vessel radius in LC as a uniform value.  
423 Currently, there are no studies offering detailed distributions of vessel radius in the LC, and the  
424 use of a uniform radius has been common in previous LC hemodynamic studies. Our  
425 reconstruction technique was based on ex-vivo histological sections. The difference in the internal  
426 environment (e.g., absence of blood pressure, interstitial fluid pressure, IOP) result in the different  
427 vessel radius from the in-vivo case. Since our analysis indicates that the vessel radius was the

428 strongest influential factor for LC oxygenation, it is important to consider the limitation of our  
429 uniform radius assumption and the potential effect due to the non-uniform radius distribution.  
430 Further research, potentially with a more advanced reconstruction technique coupled with in vivo  
431 imaging, could help provide detailed information on in-vivo LC vessel radius and estimate the  
432 effect of the radius distribution.

433 Another limitation is that our work only considers the static status of LC hemodynamics and  
434 oxygenation. All the parameters in our model were assumed to be time-invariant and independent.  
435 However, in-vivo blood/oxygen supply involves several regulation mechanisms to meet the  
436 changing demand of organisms. For instance, short-term blood flow autoregulation has been  
437 identified as a significant factor in hemodynamics and oxygenation for eye.<sup>18, 76</sup> Long-term vessel  
438 remodeling in the LC has also been reported in the development of glaucoma.<sup>2, 8</sup> Although the  
439 precise regulation and remodeling in LC remain unknown, we acknowledge that they could alter  
440 the LC blood and oxygen supply.<sup>10, 18, 20, 76-78</sup> Future research should incorporate the dynamic  
441 aspects of the LC blood and oxygen supply, which might contribute to the development of  
442 pathology, such as glaucoma.

443 It is important to note that the LC and ONH in vivo are not static. Tissue distortions, for example  
444 due to changes in IOP or gaze, can deform the vessels, affecting hemodynamics and potentially  
445 oxygenation. We recognize that such distortions can have a major impact and have thus explored  
446 them in a dedicated manuscript.<sup>79</sup> Specifically, using experimentally-derived IOP-related  
447 distortions measured using optical coherence tomography and digital volume correlation, we  
448 found that moderately elevated IOP can cause LC vessel distortions that reduce oxygenation and  
449 can even lead to mild hypoxia in a substantial part of the LC. For extreme IOP elevations, severe  
450 hypoxia was predicted.<sup>79</sup> We have also used ultrasound techniques to explore the reductions on  
451 LC oxygenation resulting from IOP effects directly on the ONH and indirectly through the posterior  
452 ciliary arteries.<sup>80</sup>

453 In summary, we used four reconstructed eye-specific 3D LC vasculature, and parameterized the  
454 vessel radius, oxygen consumption rate, and arteriole perfusion pressure in our hemodynamic  
455 models to evaluate their impact on LC oxygen supply. Our model predicted that the vessel radius  
456 and eye variation had the most significant influence on the LC oxygen supply. Situations that alter  
457 the radius, such as IOP-induced deformation, may contribute to compromised LC oxygenation.  
458 But different individuals could also exhibit different susceptibility to those pathological scenarios  
459 due to their anatomy differences.

#### 460 **Acknowledgements**

461 National Institutes of Health R01-EY023966, R01-EY031708, R01-HD083383, P30-EY008098  
462 and T32-EY017271 (Bethesda, MD), the Eye and Ear Foundation (Pittsburgh, PA), Research to  
463 Prevent Blindness (unrestricted grant to UPMC ophthalmology, and Stein innovation award to  
464 Sigal IA) and BrightFocus Foundation.

465

- 467 (1) Quigley, H.; Anderson, D. R. The dynamics and location of axonal transport blockade by acute  
468 intraocular pressure elevation in primate optic nerve. *Investigative ophthalmology & visual science* **1976**,  
469 *15* (8), 606-616.
- 470 (2) Quigley, H. A.; Nickells, R. W.; Kerrigan, L. A.; Pease, M. E.; Thibault, D. J.; Zack, D. J. Retinal ganglion  
471 cell death in experimental glaucoma and after axotomy occurs by apoptosis. *Investigative ophthalmology*  
472 *& visual science* **1995**, *36* (5), 774-786.
- 473 (3) Howell, G. R.; Libby, R. T.; Jakobs, T. C.; Smith, R. S.; Phalan, F. C.; Barter, J. W.; Barbay, J. M.; Marchant,  
474 J. K.; Mahesh, N.; Porciatti, V. Axons of retinal ganglion cells are insulted in the optic nerve early in DBA/2J  
475 glaucoma. *The Journal of cell biology* **2007**, *179* (7), 1523-1537.
- 476 (4) Quigley, H. vol. 377. *Glaucoma Lancet* **2011**, 1367-1377.
- 477 (5) Fortune, B.; Reynaud, J.; Hardin, C.; Wang, L.; Sigal, I. A.; Burgoyne, C. F. Experimental glaucoma causes  
478 optic nerve head neural rim tissue compression: a potentially important mechanism of axon injury.  
479 *Investigative ophthalmology & visual science* **2016**, *57* (10), 4403-4411.
- 480 (6) Kasi, A.; Faiq, M. A.; Chan, K. C. In vivo imaging of structural, metabolic and functional brain changes  
481 in glaucoma. *Neural Regeneration Research* **2019**, *14* (3), 446-449.
- 482 (7) Brazile, B. L.; Yang, B.; Waxman, S.; Lam, P.; Voorhees, A. P.; Hua, Y.; Loewen, R. T.; Loewen, N. A.;  
483 Rizzo, J. F.; Jakobs, T. Lamina cribrosa capillaries straighten as intraocular pressure increases. *Investigative*  
484 *Ophthalmology & Visual Science* **2020**, *61* (12), 2-2.
- 485 (8) Hayreh, S. The optic nerve head circulation in health and disease. *Ophthalmic Literature* **1996**, *2* (49),  
486 111.
- 487 (9) Levitzky, M.; Henkind, P. Angioarchitecture of the optic nerve: II. Lamina cribrosa. *American journal of*  
488 *ophthalmology* **1969**, *68* (6), 986-996.
- 489 (10) Mackenzie, P. J.; Cioffi, G. A. Vascular anatomy of the optic nerve head. *Canadian Journal of*  
490 *Ophthalmology* **2008**, *43* (3), 308-312.
- 491 (11) Sugiyama, K.; Bacon, D.; Morrison, J.; Van Buskirk, E. Optic nerve head microvasculature of the rabbit  
492 eye. *Investigative ophthalmology & visual science* **1992**, *33* (7), 2251-2261.
- 493 (12) Hamasaki, D.; Fujino, T. Effect of intraocular pressure on ocular vessels: Filling with India ink. *Archives*  
494 *of Ophthalmology* **1967**, *78* (3), 369-379.
- 495 (13) Burgoyne, C. F.; Downs, J. C.; Bellezza, A. J.; Suh, J.-K. F.; Hart, R. T. The optic nerve head as a  
496 biomechanical structure: a new paradigm for understanding the role of IOP-related stress and strain in  
497 the pathophysiology of glaucomatous optic nerve head damage. *Progress in retinal and eye research* **2005**,  
498 *24* (1), 39-73.
- 499 (14) Chuangsuwanich, T.; Birgersson, K. E.; Thiery, A.; Thakku, S. G.; Leo, H. L.; Girard, M. J. Factors  
500 influencing lamina cribrosa microcapillary hemodynamics and oxygen concentrations. *Investigative*  
501 *ophthalmology & visual science* **2016**, *57* (14), 6167-6179.
- 502 (15) Chuangsuwanich, T.; Hung, P. T.; Wang, X.; Liang, L. H.; Schmetterer, L.; Boote, C.; Girard, M. J. A.  
503 Morphometric, hemodynamic, and biomechanical factors influencing blood flow and oxygen  
504 concentration in the human lamina cribrosa. *Investigative ophthalmology & visual science* **2020**, *61* (4), 3-  
505 3.
- 506 (16) Sigal, I. A.; Grimm, J. L. A few good responses: which mechanical effects of IOP on the ONH to study?  
507 *Investigative ophthalmology & visual science* **2012**, *53* (7), 4270-4278.
- 508 (17) Sigal, I. A. Interactions between geometry and mechanical properties on the optic nerve head.  
509 *Investigative ophthalmology & visual science* **2009**, *50* (6), 2785-2795.
- 510 (18) Wang, L.; Burgoyne, C. F.; Cull, G.; Thompson, S.; Fortune, B. Static blood flow autoregulation in the  
511 optic nerve head in normal and experimental glaucoma. *Investigative Ophthalmology & Visual Science*  
512 **2014**, *55* (2), 873-880.
- 513 (19) Pitha, I.; Du, L.; Nguyen, T.; Quigley, H. IOP and glaucoma damage: The essential role of optic nerve  
514 head and retinal mechanosensors. *Progress in Retinal and Eye Research* **2023**, 101232.

515 (20) Hayreh, S. S. Blood flow in the optic nerve head and factors that may influence it. *Progress in retinal*  
516 *and eye research* **2001**, *20* (5), 595-624.

517 (21) Carichino, L.; Guidoboni, G.; Arieli, Y.; Siesky, B. A.; Harris, A. Effect of lamina cribrosa deformation on  
518 the hemodynamics of the central retinal artery: a mathematical model. *Investigative Ophthalmology &*  
519 *Visual Science* **2012**, *53* (14), 2836-2836.

520 (22) Fechtner, R. D.; Weinreb, R. N. Mechanisms of optic nerve damage in primary open angle glaucoma.  
521 *Survey of ophthalmology* **1994**, *39* (1), 23-42.

522 (23) Quigley, H. A.; McKinnon, S. J.; Zack, D. J.; Pease, M. E.; Kerrigan–Baumrind, L. A.; Kerrigan, D. F.;  
523 Mitchell, R. S. Retrograde axonal transport of BDNF in retinal ganglion cells is blocked by acute IOP  
524 elevation in rats. *Investigative ophthalmology & visual science* **2000**, *41* (11), 3460-3466.

525 (24) Lu, Y.; Hua, Y.; Wang, B.; Zhong, F.; Theophanous, A.; Tahir, S.; Lee, P.-Y.; Sigal, I. A. The Robust Lamina  
526 Cribrosa Vasculature: Perfusion and Oxygenation Under Elevated Intraocular Pressure. *Investigative*  
527 *Ophthalmology & Visual Science* **2024**, *65* (5), 1-1. DOI: 10.1167/iov.65.5.1 (accessed 5/2/2024).

528 (25) Racette, L.; Wilson, M. R.; Zangwill, L. M.; Weinreb, R. N.; Sample, P. A. Primary open-angle glaucoma  
529 in blacks: a review. *Survey of ophthalmology* **2003**, *48* (3), 295-313.

530 (26) Mari, J. M.; Strouthidis, N. G.; Park, S. C.; Girard, M. J. Enhancement of lamina cribrosa visibility in  
531 optical coherence tomography images using adaptive compensation. *Investigative ophthalmology &*  
532 *visual science* **2013**, *54* (3), 2238-2247.

533 (27) Numa, S.; Akagi, T.; Uji, A.; Suda, K.; Nakanishi, H.; Kameda, T.; Ikeda, H. O.; Tsujikawa, A. Visualization  
534 of the lamina cribrosa microvasculature in normal and glaucomatous eyes: a swept-source optical  
535 coherence tomography angiography study. *Journal of Glaucoma* **2018**, *27* (11), 1032-1035.

536 (28) Pi, S.; Hormel, T. T.; Wei, X.; Cepurna, W.; Wang, B.; Morrison, J. C.; Jia, Y. Retinal capillary oximetry  
537 with visible light optical coherence tomography. *Proceedings of the National Academy of Sciences* **2020**,  
538 *117* (21), 11658-11666.

539 (29) Rao, H. L.; Pradhan, Z. S.; Weinreb, R. N.; Riyazuddin, M.; Dasari, S.; Venugopal, J. P.; Puttaiah, N. K.;  
540 Rao, D. A.; Devi, S.; Mansouri, K. A comparison of the diagnostic ability of vessel density and structural  
541 measurements of optical coherence tomography in primary open angle glaucoma. *PloS one* **2017**, *12* (3),  
542 e0173930.

543 (30) Qian, X.; Kang, H.; Li, R.; Lu, G.; Du, Z.; Shung, K. K.; Humayun, M. S.; Zhou, Q. In vivo visualization of  
544 eye vasculature using super-resolution ultrasound microvessel imaging. *IEEE Transactions on Biomedical*  
545 *Engineering* **2020**, *67* (10), 2870-2880.

546 (31) Li, Y.; Cheng, H.; Duong, T. Q. Blood-flow magnetic resonance imaging of the retina. *Neuroimage* **2008**,  
547 *39* (4), 1744-1751.

548 (32) Sugiyama, T.; Araie, M.; Riva, C. E.; Schmetterer, L.; Orgul, S. Use of laser speckle flowgraphy in ocular  
549 blood flow research. *Acta ophthalmologica* **2010**, *88* (7), 723-729.

550 (33) Causin, P.; Guidoboni, G.; Harris, A.; Prada, D.; Sacco, R.; Terragni, S. A poroelastic model for the  
551 perfusion of the lamina cribrosa in the optic nerve head. *Mathematical biosciences* **2014**, *257*, 33-41.

552 (34) Hua, Y.; Lu, Y.; Walker, J.; Lee, P.-Y.; Tian, Q.; McDonald, H.; Pallares, P.; Ji, F.; Brazile, B. L.; Yang, B.  
553 Eye-specific 3D modeling of factors influencing oxygen concentration in the lamina cribrosa. *Experimental*  
554 *Eye Research* **2022**, 109105.

555 (35) Lee, P.-Y.; Hua, Y.; Brazile, B. L.; Yang, B.; Wang, L.; Sigal, I. A. A Workflow for Three-Dimensional  
556 Reconstruction and Quantification of the Monkey Optic Nerve Head Vascular Network. *Journal of*  
557 *Biomechanical Engineering* **2022**, *144* (6), 061006.

558 (36) Waxman, S.; Brazile, B. L.; Yang, B.; Lee, P.-Y.; Hua, Y.; Gogola, A. L.; Lam, P.; Voorhees, A. P.; Rizzo III,  
559 J. F.; Jakobs, T. C. Lamina cribrosa vessel and collagen beam networks are distinct. *Experimental Eye*  
560 *Research* **2022**, *215*, 108916.

561 (37) Tran, H.; Jan, N.-J.; Hu, D.; Voorhees, A.; Schuman, J. S.; Smith, M. A.; Wollstein, G.; Sigal, I. A. Formalin  
562 fixation and cryosectioning cause only minimal changes in shape or size of ocular tissues. *Scientific reports*  
563 **2017**, *7* (1), 1-11.

564 (38) Jan, N.-J.; Grimm, J. L.; Tran, H.; Lathrop, K. L.; Wollstein, G.; Bilonick, R. A.; Ishikawa, H.; Kagemann,  
565 L.; Schuman, J. S.; Sigal, I. A. Polarization microscopy for characterizing fiber orientation of ocular tissues.  
566 *Biomedical optics express* **2015**, *6* (12), 4705-4718.

567 (39) An, D.; Pulford, R.; Morgan, W. H.; Yu, D.-Y.; Balaratnasingam, C. Associations between capillary  
568 diameter, capillary density, and microaneurysms in diabetic retinopathy: A high-resolution confocal  
569 microscopy study. *Translational vision science & technology* **2021**, *10* (2), 6-6.

570 (40) Lu, Y.; Hu, D.; Ying, W. A fast numerical method for oxygen supply in tissue with complex blood vessel  
571 network. *PLoS one* **2021**, *16* (2), e0247641.

572 (41) Secomb, T. W.; Hsu, R.; Park, E. Y.; Dewhirst, M. W. Green's function methods for analysis of oxygen  
573 delivery to tissue by microvascular networks. *Annals of biomedical engineering* **2004**, *32* (11), 1519-1529.

574 (42) Pries, A. R.; Secomb, T.; Gessner, T.; Sperandio, M.; Gross, J.; Gaehtgens, P. Resistance to blood flow  
575 in microvessels in vivo. *Circulation research* **1994**, *75* (5), 904-915.

576 (43) Mozaffarieh, M.; Bärtschi, M.; Henrich, P.; Schoetzau, A.; Flammer, J. Retinal venous pressure in the  
577 non-affected eye of patients with retinal vein occlusions. *Graefes Archive for Clinical and Experimental*  
578 *Ophthalmology* **2014**, *252* (10), 1569-1571.

579 (44) Causin, P.; Guidoboni, G.; Malgaroli, F.; Sacco, R.; Harris, A. Blood flow mechanics and oxygen  
580 transport and delivery in the retinal microcirculation: multiscale mathematical modeling and numerical  
581 simulation. *Biomechanics and modeling in mechanobiology* **2016**, *15* (3), 525-542.

582 (45) Sigal, I. A.; Lee, P.-Y.; Quinn, M.; Waxman, S.; Voorhees, A. P.; Yang, B.; Jakobs, T. C.; Rizzo, J.; Fortune,  
583 B.; Hua, Y. The lamina cribrosa vascular network is heavily interconnected with that of adjacent regions,  
584 not just the periphery, likely improving perfusion resilience. *Investigative Ophthalmology & Visual Science*  
585 **2022**, *63* (7), 4031–A0416-4031–A0416.

586 (46) Morgan, W. H.; Yu, D.-Y.; Alder, V. A.; Cringle, S. J.; Cooper, R. L.; House, P. H.; Constable, I. J. The  
587 correlation between cerebrospinal fluid pressure and retrolaminar tissue pressure. *Investigative*  
588 *ophthalmology & visual science* **1998**, *39* (8), 1419-1428.

589 (47) Roberts, M. D.; Liang, Y.; Sigal, I. A.; Grimm, J.; Reynaud, J.; Bellezza, A.; Burgoyne, C. F.; Downs, J. C.  
590 Correlation between local stress and strain and lamina cribrosa connective tissue volume fraction in  
591 normal monkey eyes. *Investigative ophthalmology & visual science* **2010**, *51* (1), 295-307.

592 (48) Feola, A. J.; Myers, J. G.; Raykin, J.; Mulugeta, L.; Nelson, E. S.; Samuels, B. C.; Ethier, C. R. Finite  
593 element modeling of factors influencing optic nerve head deformation due to intracranial pressure.  
594 *Investigative ophthalmology & visual science* **2016**, *57* (4), 1901-1911.

595 (49) Hua, Y.; Voorhees, A. P.; Sigal, I. A. Cerebrospinal fluid pressure: revisiting factors influencing optic  
596 nerve head biomechanics. *Investigative ophthalmology & visual science* **2018**, *59* (1), 154-165.

597 (50) Wang, Y.; Lu, A.; Gil-Flamer, J.; Tan, O.; Izatt, J. A.; Huang, D. Measurement of total blood flow in the  
598 normal human retina using Doppler Fourier-domain optical coherence tomography. *British Journal of*  
599 *Ophthalmology* **2009**, *93* (5), 634-637.

600 (51) Ul Banna, H.; Mitchell, B.; Chen, S.; Palko, J. Super-Resolution Ultrasound Localization Microscopy  
601 Using High-Frequency Ultrasound to Measure Ocular Perfusion Velocity in the Rat Eye. *Bioengineering*  
602 **2023**, *10* (6), 689.

603 (52) Guidoboni, G.; Harris, A.; Cassani, S.; Arciero, J.; Siesky, B.; Amireskandari, A.; Tobe, L.; Egan, P.;  
604 Januleviciene, I.; Park, J. Intraocular pressure, blood pressure, and retinal blood flow autoregulation: a  
605 mathematical model to clarify their relationship and clinical relevance. *Investigative ophthalmology &*  
606 *visual science* **2014**, *55* (7), 4105-4118.

607 (53) Davies, A. L.; Desai, R. A.; Bloomfield, P. S.; McIntosh, P. R.; Chapple, K. J.; Lington, C.; Fairless, R.;  
608 Diem, R.; Kastl, M.; Murphy, M. P. Neurological deficits caused by tissue hypoxia in neuroinflammatory  
609 disease. *Annals of neurology* **2013**, *74* (6), 815-825.

610 (54) McKeown, S. Defining normoxia, physoxia and hypoxia in tumours—implications for treatment  
611 response. *The British journal of radiology* **2014**, *87* (1035), 20130676.

612 (55) Ortiz-Prado, E.; Natah, S.; Srinivasan, S.; Dunn, J. F. A method for measuring brain partial pressure of  
613 oxygen in unanesthetized unrestrained subjects: the effect of acute and chronic hypoxia on brain tissue  
614 PO<sub>2</sub>. *Journal of neuroscience methods* **2010**, *193* (2), 217-225.

615 (56) Leach, R.; Treacher, D. Oxygen transport<sup>2</sup>. Tissue hypoxia. *Bmj* **1998**, *317* (7169), 1370-1373.

616 (57) Ortiz-Prado, E.; Dunn, J. F.; Vasconez, J.; Castillo, D.; Viscor, G. Partial pressure of oxygen in the human  
617 body: a general review. *American journal of blood research* **2019**, *9* (1), 1.

618 (58) Erecińska, M.; Silver, I. A. Tissue oxygen tension and brain sensitivity to hypoxia. *Respiration*  
619 *physiology* **2001**, *128* (3), 263-276.

620 (59) Beach, J.; Ning, J.; Khoobehi, B. Oxygen saturation in optic nerve head structures by hyperspectral  
621 image analysis. *Current Eye Research* **2007**, *32* (2), 161-170.

622 (60) De Filippis, L.; Delia, D. Hypoxia in the regulation of neural stem cells. *Cellular and Molecular Life*  
623 *Sciences* **2011**, *68* (17), 2831-2844.

624 (61) Hockel, M.; Vaupel, P. Tumor hypoxia: definitions and current clinical, biologic, and molecular aspects.  
625 *Journal of the National Cancer Institute* **2001**, *93* (4), 266-276.

626 (62) Carreau, A.; Hafny-Rahbi, B. E.; Matejuk, A.; Grillon, C.; Kieda, C. Why is the partial oxygen pressure  
627 of human tissues a crucial parameter? Small molecules and hypoxia. *Journal of cellular and molecular*  
628 *medicine* **2011**, *15* (6), 1239-1253.

629 (63) Ferrez, P.; Chamot, S.; Petrig, B.; Pournaras, C.; Riva, C. Effect of visual stimulation on blood  
630 oxygenation in the optic nerve head of miniature pigs: a pilot study. *Klinische Monatsblätter für*  
631 *Augenheilkunde* **2004**, *221* (05), 364-366.

632 (64) Boltz, A.; Schmidl, D.; Werkmeister, R. M.; Lasta, M.; Kaya, S.; Palkovits, S.; Told, R.; Napora, K. J.;  
633 Popa-Cherecheanu, A.; Garhöfer, G. Regulation of optic nerve head blood flow during combined changes  
634 in intraocular pressure and arterial blood pressure. *Journal of Cerebral Blood Flow & Metabolism* **2013**, *33*  
635 (12), 1850-1856.

636 (65) Kiyota, N.; Shiga, Y.; Ichinohasama, K.; Yasuda, M.; Aizawa, N.; Omodaka, K.; Honda, N.; Kunikata, H.;  
637 Nakazawa, T. The impact of intraocular pressure elevation on optic nerve head and choroidal blood flow.  
638 *Investigative Ophthalmology & Visual Science* **2018**, *59* (8), 3488-3496.

639 (66) Iwase, T.; Akahori, T.; Yamamoto, K.; Ra, E.; Terasaki, H. Evaluation of optic nerve head blood flow in  
640 response to increase of intraocular pressure. *Scientific reports* **2018**, *8* (1), 17235.

641 (67) Lu, Y.; Hua, Y.; Wang, B.; Zhong, F.; Theophanous, A.; Tahir, S.; Lee, P.-Y.; Sigal, I. A. Moderately  
642 elevated IOP may alter optic nerve head hemodynamics enough to cause mild hypoxia over a substantial  
643 part of the lamina cribrosa. *Investigative Ophthalmology & Visual Science* **2023**, *64* (8), 4732-4732.  
644 (accessed 8/14/2024).

645 (68) Voorhees, A.; Hua, Y.; Sigal, I.; Roberts, C.; Dupps, W.; Downs, C. Parametric analysis to identify  
646 biomechanical risk factors; taking control of population diversity and experiment variability. *Roberts CJ,*  
647 *Dupps WJ, Downs C. Biomechanics of the Eye. Amsterdam, The Netherlands: Kugler Publications* **2018**.

648 (69) Hayreh, S. S.; Zimmerman, M. B.; Podhajsky, P.; Alward, W. L. Nocturnal arterial hypotension and its  
649 role in optic nerve head and ocular ischemic disorders. *American journal of ophthalmology* **1994**, *117* (5),  
650 603-624.

651 (70) Graham, S. L.; Drance, S. M.; Wijsman, K.; Douglas, G. R.; Mikelberg, F. S. Ambulatory blood pressure  
652 monitoring in glaucoma: the nocturnal dip. *Ophthalmology* **1995**, *102* (1), 61-69.

653 (71) Dielemans, I.; Vingerling, J. R.; Algra, D.; Hofman, A.; Grobbee, D. E.; de Jong, P. T. Primary open-angle  
654 glaucoma, intraocular pressure, and systemic blood pressure in the general elderly population: the  
655 Rotterdam Study. *Ophthalmology* **1995**, *102* (1), 54-60.

656 (72) Hulsman, C. A.; Vingerling, J. R.; Hofman, A.; Witteman, J. C.; de Jong, P. T. Blood pressure, arterial  
657 stiffness, and open-angle glaucoma: the Rotterdam study. *Archives of ophthalmology* **2007**, *125* (6), 805-  
658 812.

659 (73) Bosch, A. J.; Harazny, J. M.; Kistner, I.; Friedrich, S.; Wojtkiewicz, J.; Schmieder, R. E. Retinal capillary  
660 rarefaction in patients with untreated mild-moderate hypertension. *BMC cardiovascular disorders* **2017**,  
661 *17*, 1-11.

662 (74) Schiffrin, E. L. Reactivity of small blood vessels in hypertension: relation with structural changes. State  
663 of the art lecture. *Hypertension* **1992**, *19* (2\_supplement), II1.

664 (75) Muraoka, Y.; Tsujikawa, A.; Kumagai, K.; Akiba, M.; Ogino, K.; Murakami, T.; Akagi-Kurashige, Y.;  
665 Miyamoto, K.; Yoshimura, N. Age-and hypertension-dependent changes in retinal vessel diameter and  
666 wall thickness: an optical coherence tomography study. *American journal of ophthalmology* **2013**, *156* (4),  
667 706-714. e702.

668 (76) Yu, J.; Liang, Y.; Thompson, S.; Cull, G.; Wang, L. Parametric transfer function analysis and modeling  
669 of blood flow autoregulation in the optic nerve head. *International Journal of Physiology, Pathophysiology*  
670 *and Pharmacology* **2014**, *6* (1), 13.

671 (77) Mozaffarieh, M.; Grieshaber, M. C.; Flammer, J. Oxygen and blood flow: players in the pathogenesis  
672 of glaucoma. *Molecular vision* **2008**, *14*, 224.

673 (78) Orgül, S.; Gugleta, K.; Flammer, J. Physiology of perfusion as it relates to the optic nerve head. *Survey*  
674 *of ophthalmology* **1999**, *43*, S17-S26.

675 (79) Lu, Y.; Hua, Y.; Wang, B.; Tian, Q.; Zhong, F.; Theophanous, A.; Tahir, S.; Lee, P.-Y.; Sigal, I. A. Impact  
676 of elevated IOP on lamina cribrosa oxygenation: A combined experimental-computational study on  
677 monkeys. *Ophthalmology Science* **2025**, 100725.

678 (80) Lu, Y.; Banna, H.; Yi, H.; Schilpp, H.; Liu, M.; Zhong, F.; Wang, B.; theophanous, A.; Tahir, S.; Lee, P.-Y.;  
679 et al. Elevated IOP reduces lamina cribrosa oxygenation both directly through capillary distortion and  
680 indirectly by reducing perfusion from the posterior ciliary arteries. *Investigative Ophthalmology & Visual*  
681 *Science* **2024**, *65* (7), 392-392. (accessed 8/12/2024).

682 (81) Pries, A. R.; Secomb, T. W. Blood flow in microvascular networks. In *Microcirculation*, Elsevier, 2008;  
683 pp 3-36.

684 (82) Lipowsky, H. H.; Usami, S.; Chien, S. In vivo measurements of “apparent viscosity” and microvessel  
685 hematocrit in the mesentery of the cat. *Microvascular research* **1980**, *19* (3), 297-319.

686 (83) Hayreh, S. S. Blood supply of the optic nerve head and its role in optic atrophy, glaucoma, and oedema  
687 of the optic disc. *The British journal of ophthalmology* **1969**, *53* (11), 721.

688 (84) Chu, Y.-C.; Chen, C.-Z.; Lee, C.-H.; Chen, C.-W.; Chang, H.-Y.; Hsiue, T.-R. Prediction of arterial blood  
689 gas values from venous blood gas values in patients with acute respiratory failure receiving mechanical  
690 ventilation. *Journal of the Formosan Medical Association* **2003**, *102* (8), 539-543.

691

692

694 **Effective viscosity**

695 The effective viscosity  $\mu$  within the blood vessel accounts for the Fåhræus-Lindqvist effect, which  
 696 describes the dependence of blood viscosity on vessel radius and hematocrit.

697 In our model, we used the same rheological parameter settings used in <sup>81</sup>. to compute effective  
 698 blood viscosity in vivo. These settings are supported by experimental data from Lipowsky <sup>82</sup>. The  
 699 effective viscosity  $\mu$  was calculated using the following formula:

$$700 \quad \mu = \left( 1 + (\mu_{0.45}^* - 1) \cdot \frac{(1 - H_D)^C - 1}{(1 - 0.45)^C - 1} \cdot \frac{r^4}{(r - 0.55)^4} \right) \cdot \mu_{plasma}$$

$$701 \quad C = (0.8 + \exp(-0.15r)) \cdot \left( -1 + \frac{1}{1 + 4 \cdot 10^{-8} * r^{12}} \right) + \frac{1}{1 + 4 \cdot 10^{-8} * r^{12}}$$

$$702 \quad \mu_{0.45}^* = 6 \cdot \exp(-0.017r) + 3.2 - 2.44 \cdot \exp(-0.094r^{0.645})$$

703 Here, the hematocrit  $H_D$  was set as 0.45, and plasma viscosity  $\mu_{plasma}$  was set as 1.0466 mpa\*s.

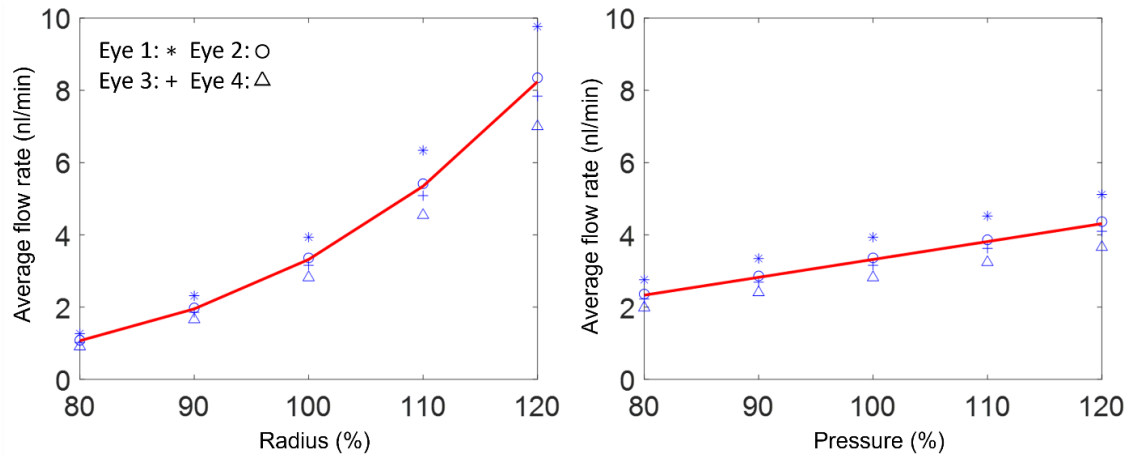
704 For a baseline vessel diameter of 8  $\mu\text{m}$ , the effective viscosity was approximately  $7.65 \times 10^{-3}$

705 mPa\*s.

706 **Flow rate across different vessel radii and pressures.**

707 Figure S1 illustrates flow rate changes as a function of radius and pressure.

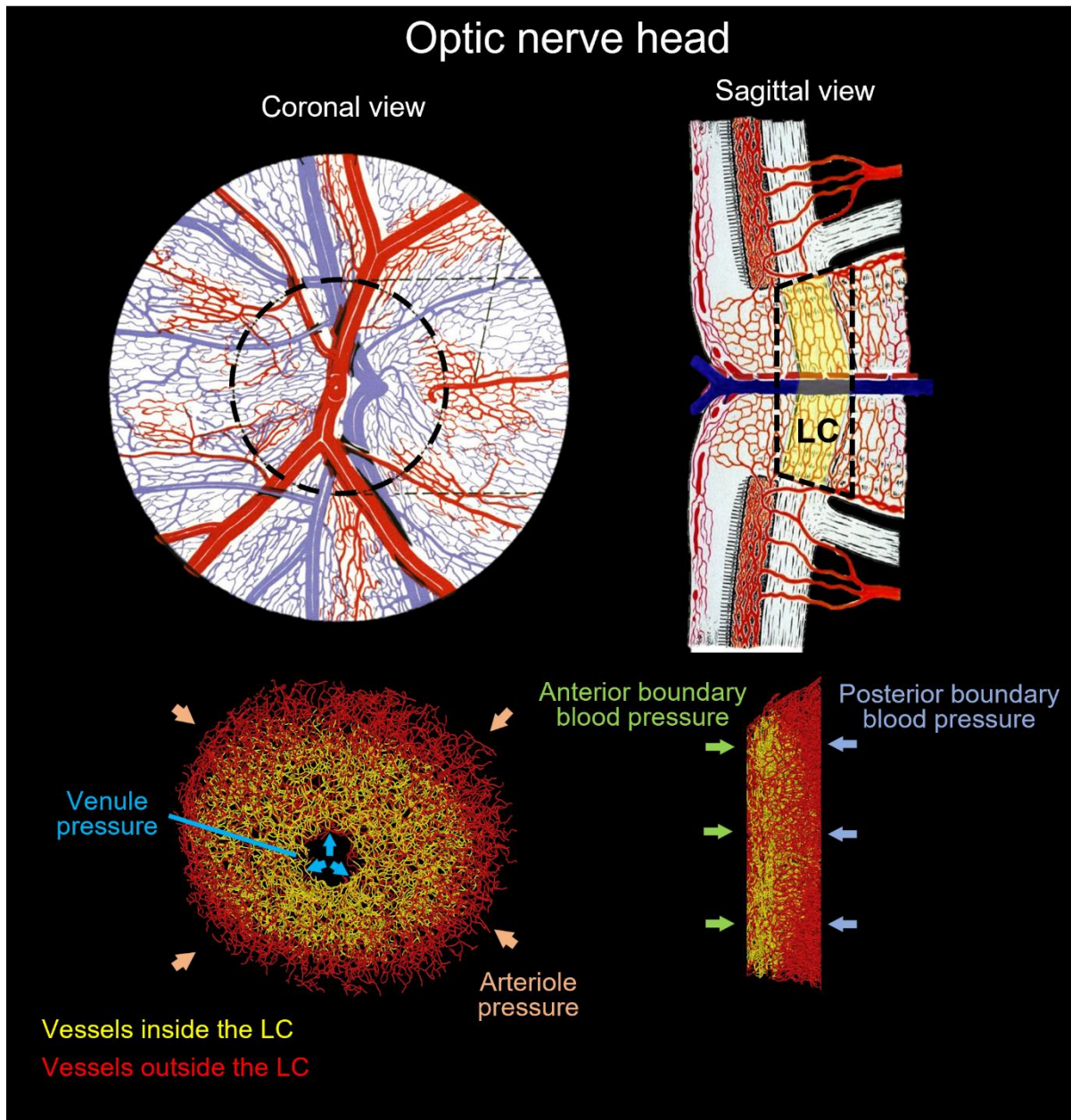
- 708 • The flow rate change slightly exceeds the fourth power of radius change, due to the fourth  
 709 order relationship in Poiseuille flow and the dependence of effective viscosity on vessel  
 710 diameter.
- 711 • The flow rate change is slightly less than the ratio of pressure difference change, as the  
 712 pressure parameter in this analysis only consider peripheral pressure, while  
 713 anterior/posterior pressure remains unchanged in this parametric study.



714 **Figure S1:** Average flow rate change as a function of radius (left) and pressure (right). The flow  
 715 rate changes slightly exceed the fourth power of the radius variation due to viscosity dependence.  
 716 Flow rate changes are slightly less than the ratio of pressure difference change, as the pressure  
 717 parameter only accounts for peripheral pressure, while anterior/posterior pressure remains  
 718 unchanged in this analysis.

720

721

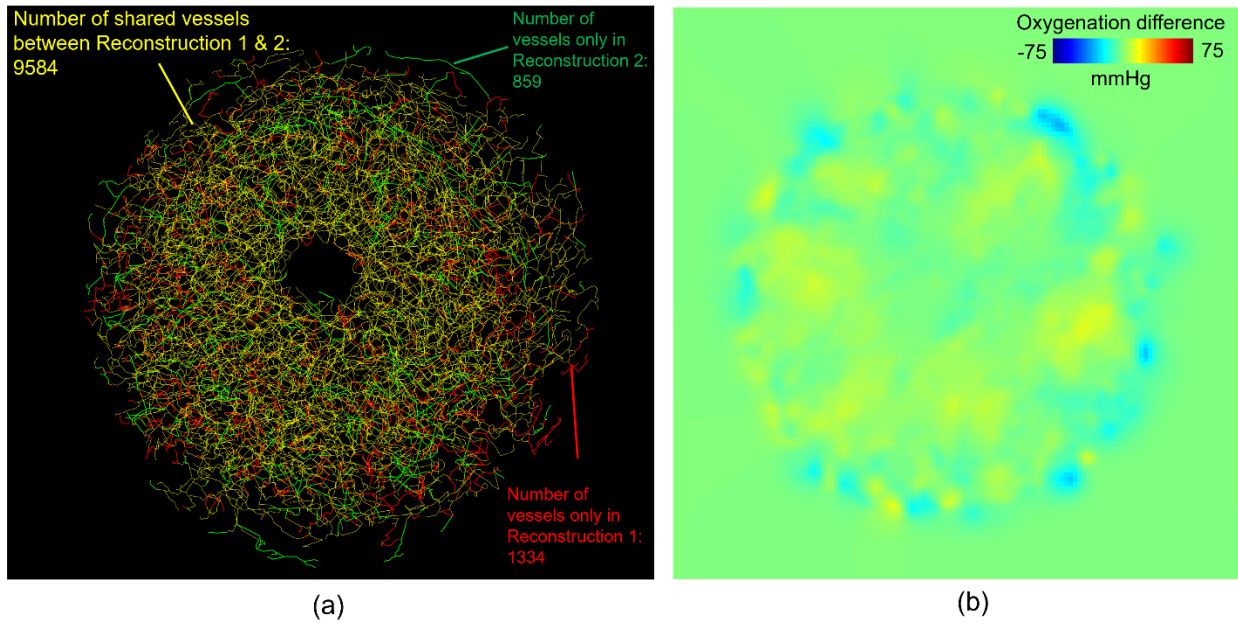


722

723 **Figure 1.** (Top) Diagram of the ONH adapted from <sup>83</sup>. Our model represents the vessels within  
 724 the scleral canal, included the whole LC region, and some of the pre-laminar and retro-laminar  
 725 regions. Black dashed lines represent the model boundaries, yellow area represents the LC  
 726 region. (Bottom) An example eye-specific vessel network. To improve flow boundary conditions  
 727 the region reconstructed extended beyond the LC. Vessels within the LC are shown colored in  
 728 yellow. Vessels reconstructed but outside the LC are shown in red. The network is labeled to  
 729 illustrate the blood pressure boundary condition settings. Four blood pressure conditions were

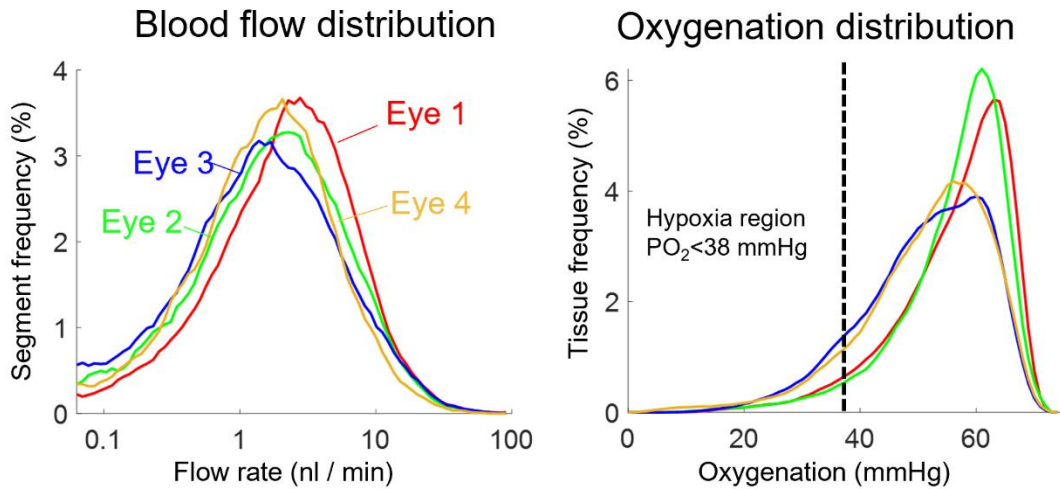
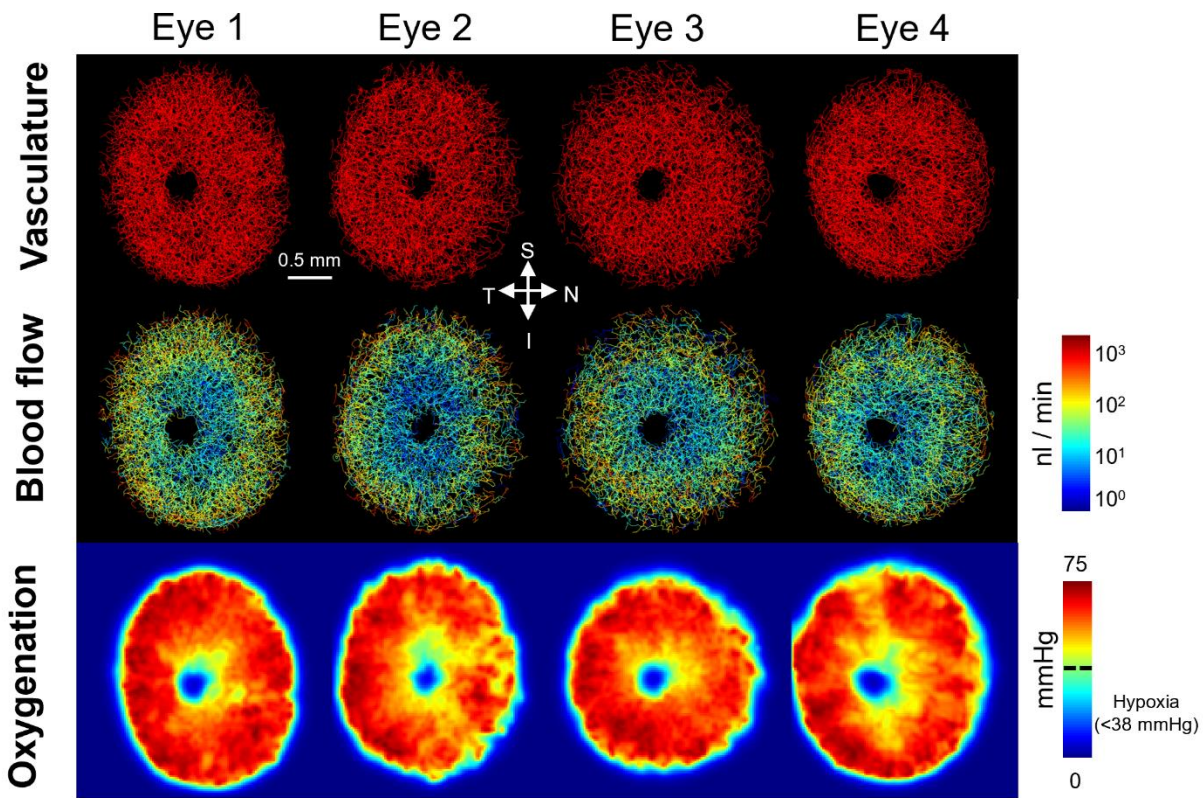
730 assigned at the peripheral, central, anterior, and posterior boundaries of the model. See the main  
731 text for the rationale and details on how these pressures were assigned.

732



733

734 **Figure 2.** Repeatability of vascular reconstruction. Two independent reconstructions of the  
735 same labeled eye showed high geometric and oxygenation consistency. (a) Over 90% of  
736 vessels were shared between the reconstructions. (b) Oxygenation differences were minimal,  
737 with an average oxygen partial pressure difference of 0.71 mmHg.



738

739 **Figure 3.** Vascular geometry, baseline hemodynamics, and baseline oxygenation of four eyes.

740 Top: Vascular geometry and maps of blood flow and oxygenation. Bottom: Distributions of blood

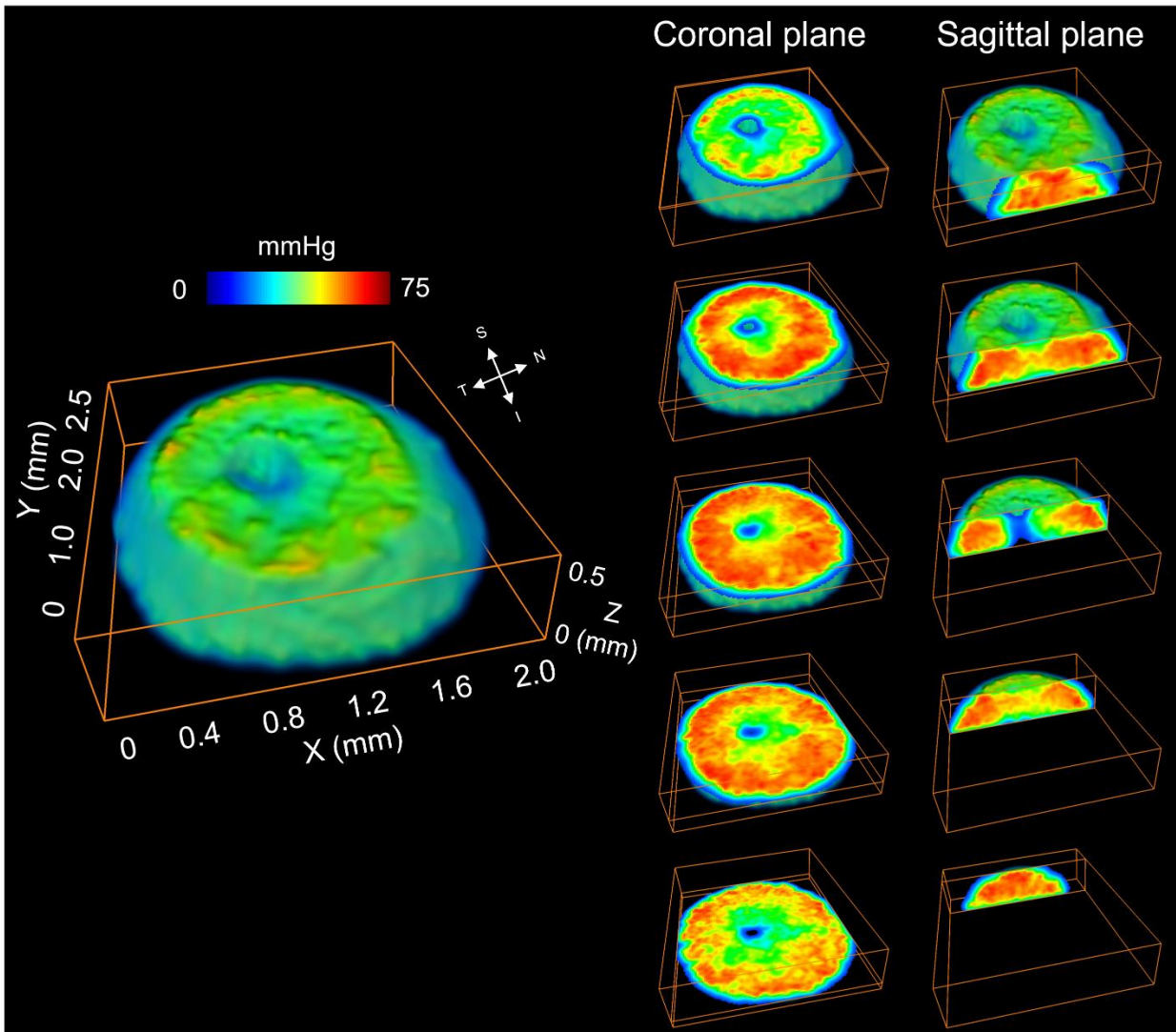
741 flow and oxygenation in the LC region. Blood flow and oxygenation exhibited similar features and

742 tendencies across all eyes. Higher flow rates and oxygenation occurred at the periphery of the

743 LC region, and lower flow rates and oxygenation were observed at the center. Interestingly, the

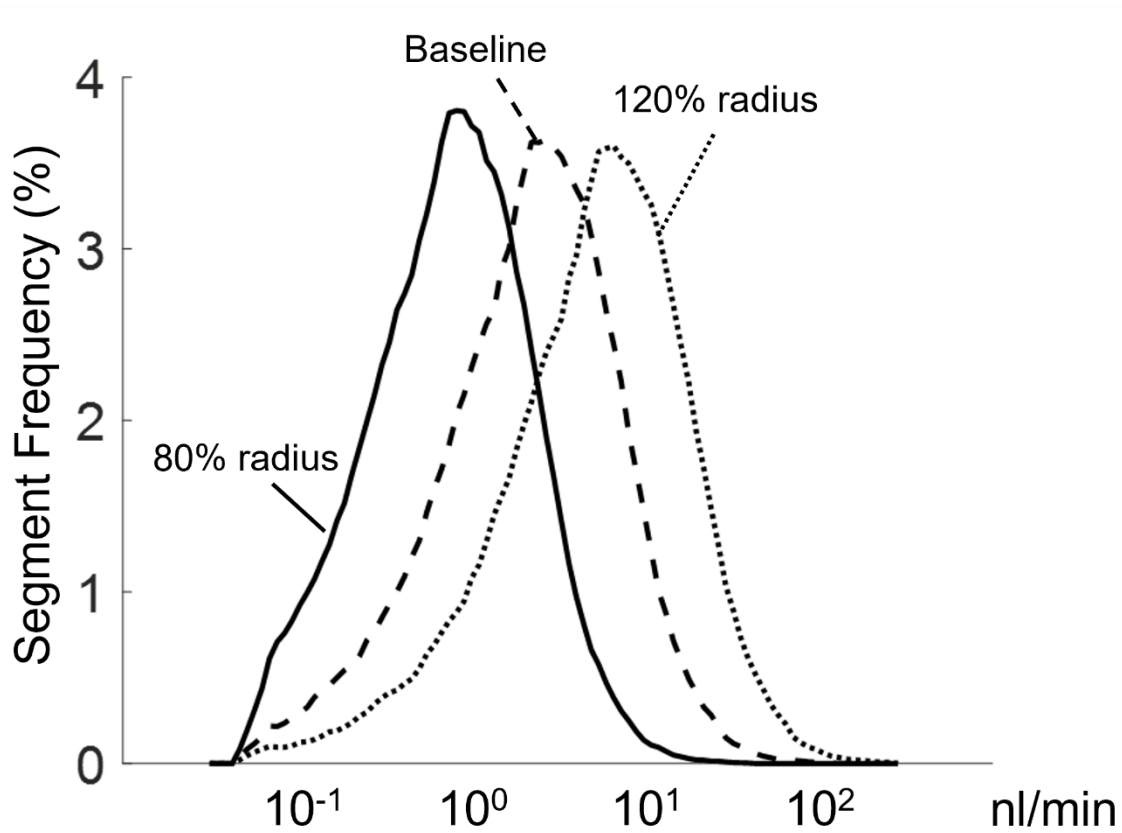
744 distribution curves of blood flow and oxygenation showed different patterns. Blood flow exhibited

745 significant variation across the entire LC, ranging from 1 to 1000 nl/min, while the LC was  
746 consistently well-provided with oxygen. Oxygen tensions remain consistently high throughout  
747 most of the LC region, with minimal regions experiencing hypoxic conditions.



748  
749 **Figure 4.** 3D oxygenation map for Eye 1 ONH. Five sections were selected for visualization in  
750 the coronal and sagittal planes. In the coronal sections, the peripheral region generally exhibits  
751 higher oxygenation levels compared to the central region. However, regions near the model  
752 boundary, such as the superficial plane or the extreme peripheral rim, also show reduced  
753 oxygenation levels. While the entire ONH model is shown, our analysis is focused on the LC  
754 region.

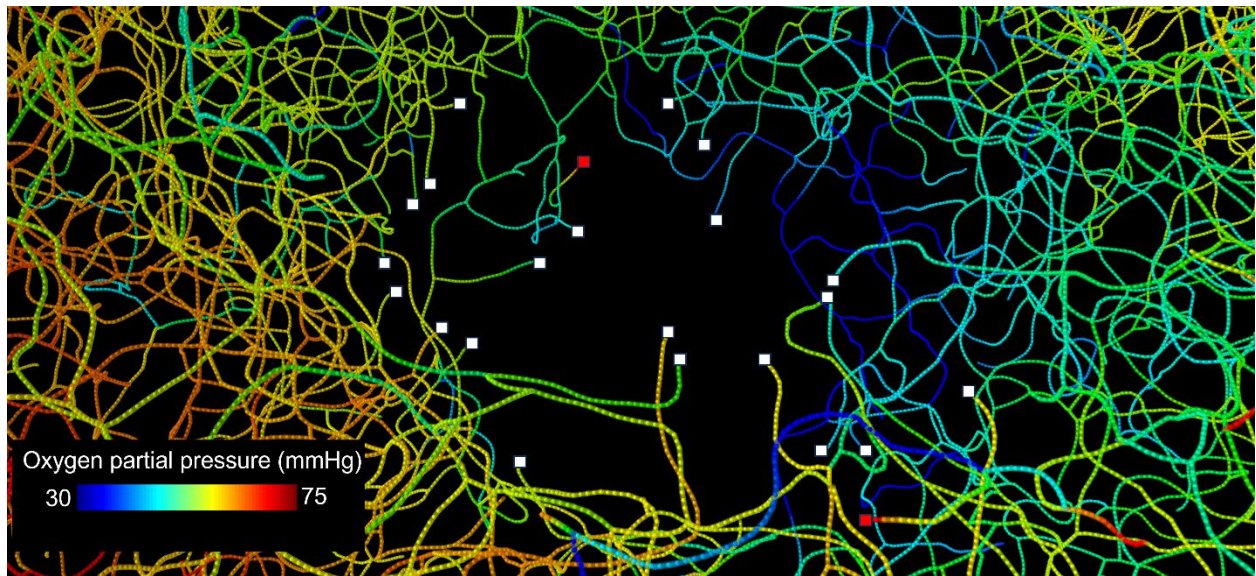
755



756

757 **Figure 5.** Flow rate distribution for Eye 1 under different radii. As expected, the flow rates increase  
 758 as the radii were larger. The average flow rates were 1.06, 3.31, and 8.23 nl/min when the radius  
 759 was adjusted to 80%, 100%, and 120% of the baseline value, respectively. Very few vessels have  
 760 ocular arterial-level flows (>45 nl/min), with 0.1% for the baseline case and 0.7% for the 120%  
 761 case.

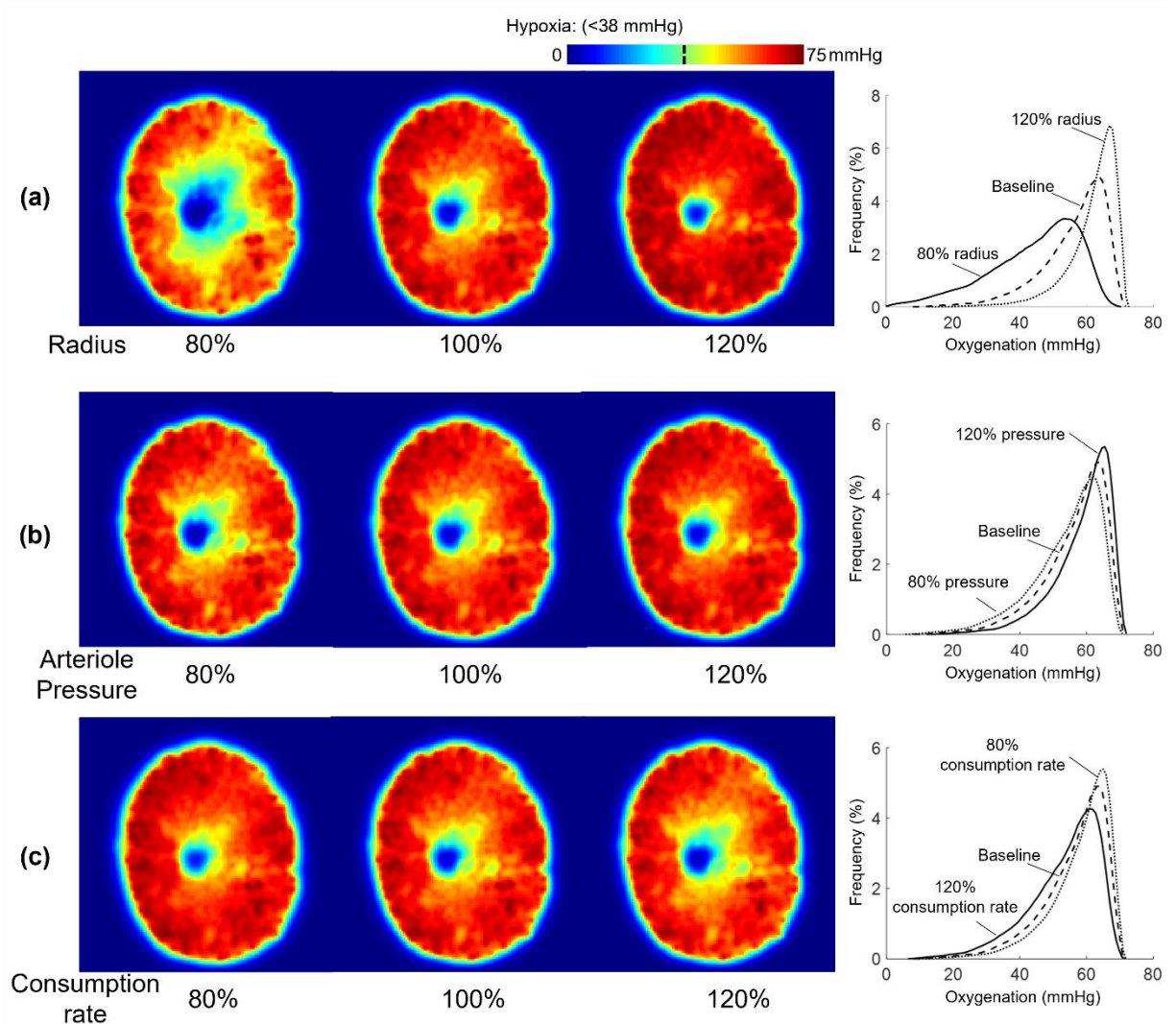
762



763

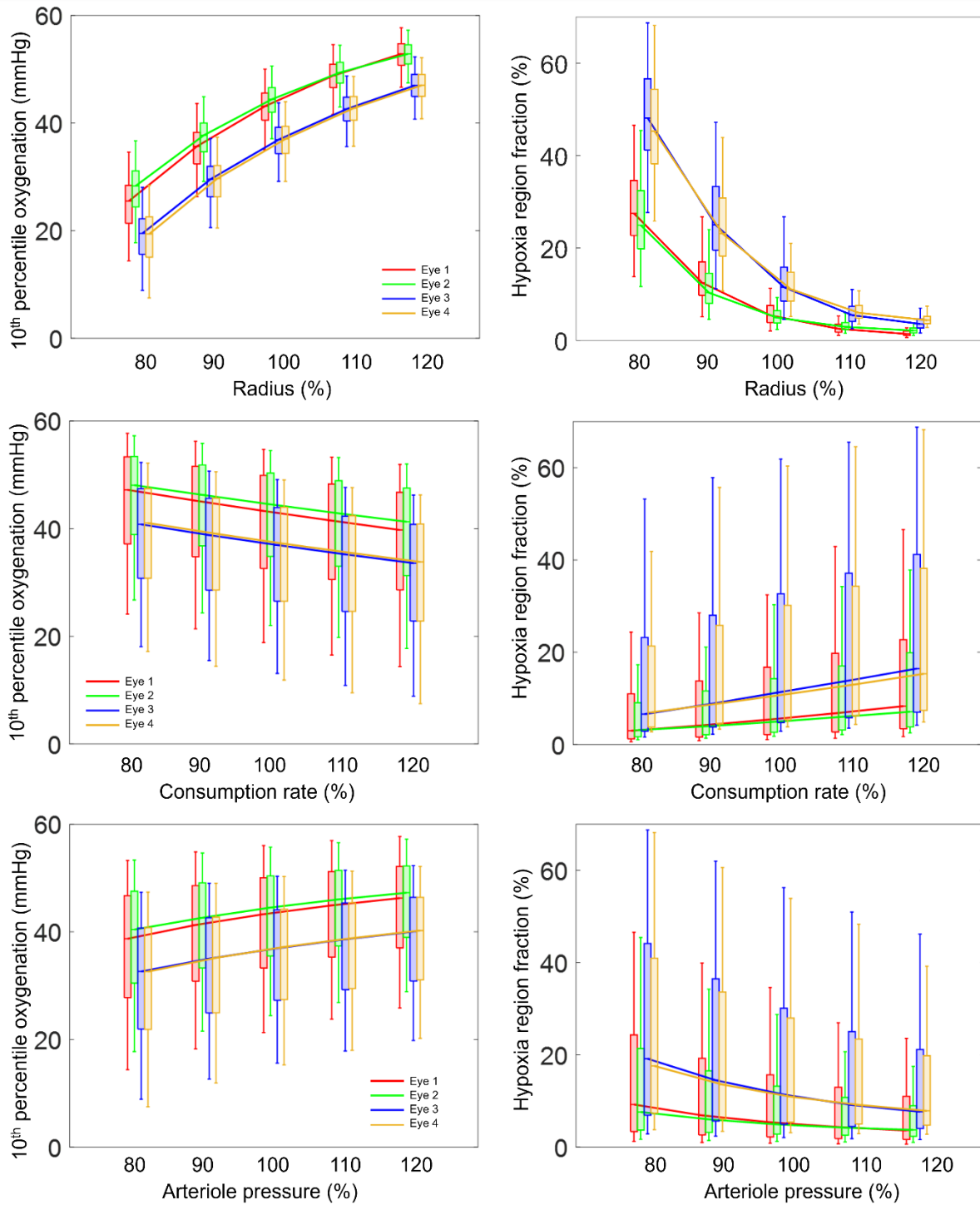
764 **Figure 6.** A screenshot of the video illustrating red blood cell transport in the blood vessels. The  
 765 region shown is a close-up of the drainage at the central retinal vessels. Colors represent the  
 766 blood oxygen saturation. The dots along each vessel represent the red blood cells. White and red  
 767 squares represent blood flow outlets and inlets, respectively. The vessel ends in the center of the  
 768 LC serve as flow outlets, according to the boundary conditions of flow drainage through the center  
 769 retinal vein. Vessel ends that are not draining are because they end at the model anterior/posterior  
 770 boundary (see Figure 1) and thus flow can be to/from the LC. Notably, the blood oxygen saturation  
 771 exhibits an asymmetric pattern at the center, with lower oxygenation observed on the right side  
 772 (Nasal side).

773



774

775 **Figure 7.** Oxygenation distribution across various radii, consumption rates, and arteriole  
 776 pressures for eye 1. (a) Oxygenation at different radii. (b) Oxygenation at different Arteriole  
 777 pressures. (c) Oxygenation at different consumption rates. Three levels—low (80%), baseline  
 778 (100%), and high (120%)—were selected to illustrate the impact of each parameter. Radius  
 779 demonstrated the strongest positive influence on oxygenation, while consumption rate and  
 780 arteriole pressure had minor effects. Most hypoxia regions were observed near the center of the  
 781 LC across all parametric scenarios.



782

783 **Figure 8.** Boxplots showing the factor influences on the 10<sup>th</sup> percentile oxygenation and hypoxia

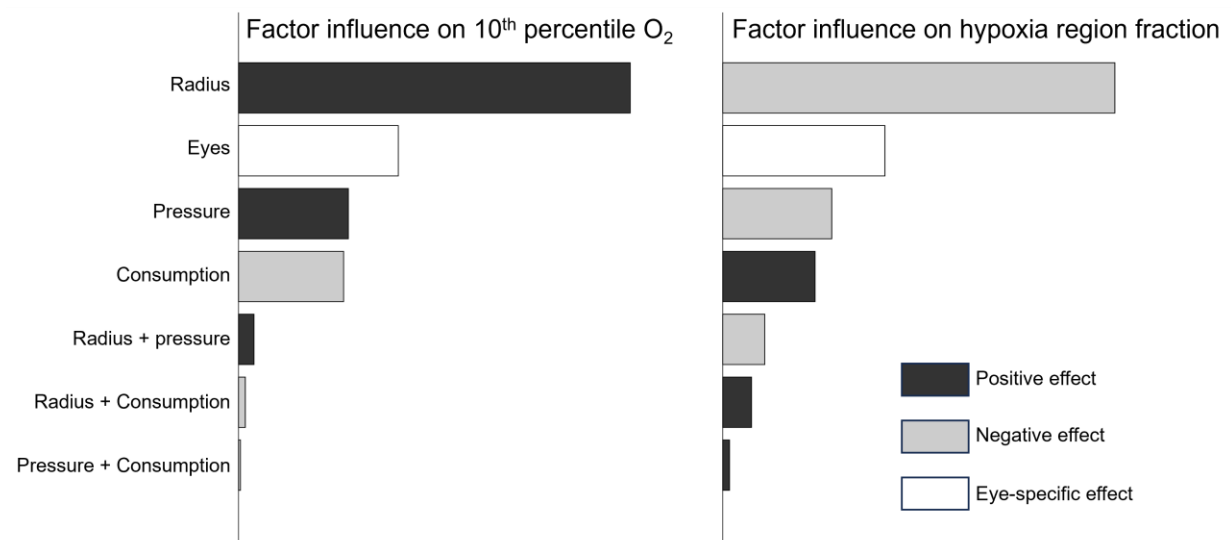
784 region fraction in the lamina cribrosa across all eyes. The top and bottom edges of each box are

785 the upper and lower quartiles (25<sup>th</sup> and 75<sup>th</sup> percentiles), while the line inside of each box is the

786 sample median (50<sup>th</sup> percentiles), respectively. The end of the whiskers shows the minimum and

787 maximum. To aid visualization we added lines connecting the median values. Vessel radius shows  
788 the strongest positive relationship with the 10th percentile oxygenation and the strongest negative  
789 relationship with the hypoxia region fraction. The variation observed among different eyes  
790 exceeds the oxygenation difference between scenarios with 80% consumption rate/arteriole  
791 pressure and those with 120% consumption rate/arteriole pressure. Interestingly, Eyes 1 and 2  
792 exhibited similar LC oxygenation across all parametric cases, while Eyes 3 and 4 also showed  
793 similar patterns to each other but differed from Eyes 1 and 2. The changes in LC oxygenation in  
794 response to the parameters, or in other words, the sensitivity to parameters, were consistent  
795 across all eyes.

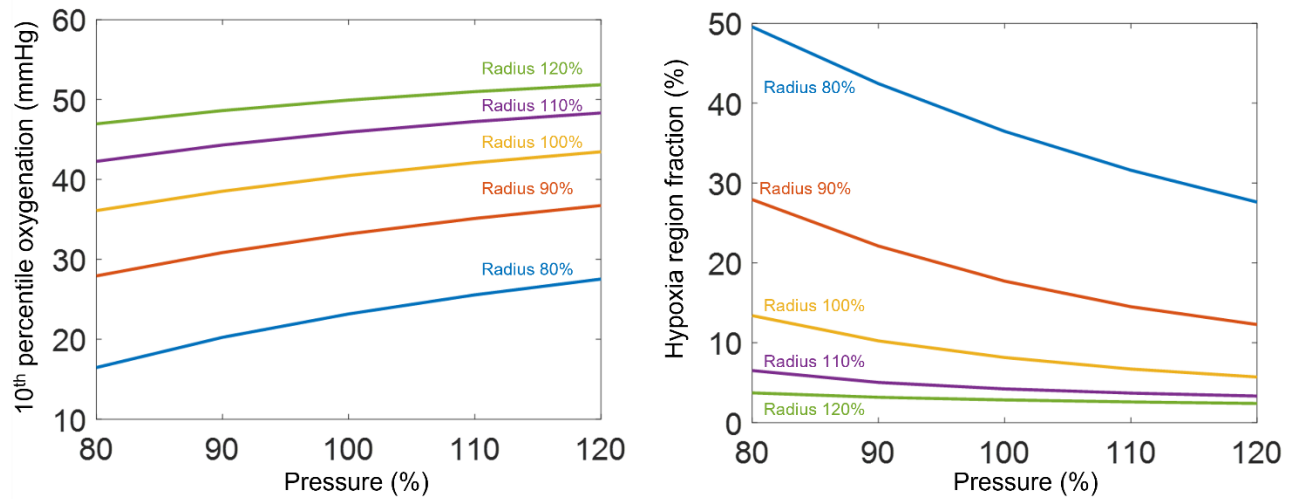
796



797

798 **Figure 9.** Bar chart showing the influence of factors and interactions on the 10th percentile  
 799 oxygenation and hypoxia region fraction in the LC, as determined by ANOVA. The factors are  
 800 listed in descending order of their influence. The vessel radius was strongest influence factor,  
 801 followed by the eye, arteriole pressure, and consumption rate. Interactions between the  
 802 parameters show minor contributions to the LC oxygenation.

803



804

805 **Figure 10.** Interactions between vessel radius and arteriole pressure on LC oxygenation.

806 Regarding the 10<sup>th</sup> percentile oxygenation, the curves for different pressures were nearly

807 parallel, suggesting a weak interaction between the radius and pressure parameters. For

808 hypoxia region fraction, the influence of the pressure was stronger when the radius was low. An

809 illustration of flow rate variations as a function of radius and pressure is provided in Appendix

810 Figure R5.

811 **Table 1. Parameters used in hemodynamic and oxygenation simulations.**

Constant parameters	Value	Reference
Oxygen diffusion coefficient, $D\alpha$	$6 \times 10^{-10}$ mlO <sub>2</sub> /cm/s/mmHg	41
Effective oxygen solubility, $\alpha_{eff}$	$3.1 \times 10^{-5}$ mlO <sub>2</sub> /ml/mmHg	41
Oxygenation at half-maximal consumption, $P_0$	10.5 mmHg	41
Maximal RBC oxygen concentration $C_0$	0.5 mlO <sub>2</sub> /ml	41
Venule pressure	15 mmHg	34
Anterior blood pressure	20 mmHg	34
Posterior blood pressure	16 mmHg	34
Effective viscosity for 4 $\mu$ m radius vessel	$7.65 \times 10^{-3}$ mPa*s	81
Inlet Blood oxygenation	75 mmHg	84
<b>Parametric factors</b>		
Vessel radius	4 $\mu$ m	34
Arteriole pressure	50 mmHg	34
Consumption rate, $M_0$	$5 \times 10^{-4}$ mlO <sub>2</sub> /ml/s	34

812

813 **Table 2.** Geometric parameters for the four eye vasculatures. The distance was defined as the  
 814 mean distance from each LC tissue point to its closest vessel. The tortuosity was calculated as  
 815 the ratio of the vessel segment path length to its end-to-end distance.

	Segment number	Branch point number	Region volume (mm <sup>3</sup> )	Total length (mm)	Average distance to nearest vessel ( $\mu$ m)	Average tortuosity
Eye 1	12966	9089	1.456	646.6	53.478	1.129
Eye 2	10918	8886	1.304	528.7	52.545	1.114
Eye 3	12012	9436	1.298	547.8	56.026	1.115
Eye 4	10700	8151	1.169	628.3	61.621	1.270

816